International Journal of Heat and Mass Transfer 220 (2024) 124901

Contents lists available at ScienceDirect

International Journal of Heat and Mass Transfer

journal homepage: www.elsevier.com/locate/ijhmt

Development of Two-Phase Frictional Pressure Gradient Correlation for Saturated Cryogenic Flow Boiling in Uniformly Heated Tubes

Vishwanath Ganesan [a], Raj Patel [a], Jason Hartwig [b], Issam Mudawar [a,1,*]

[a] Purdue University Boiling and Two-Phase Flow Laboratory (PU-BTPFL), School of Mechanical Engineering, Purdue University, 585 Purdue Mall, West Lafayette, IN 47907, USA
[b] NASA Glenn Research Center, Fluids and Cryogenics Branch, Cleveland, OH 44135, USA

ARTICLE INFO

Keywords:
Cryogens
Two-phase frictional pressure gradient
Saturated flow boiling
Adiabatic liquid-vapor flow
Dispersed flow
Separated flow

ABSTRACT

Experiments to determine two-phase frictional pressure drop for saturated cryogenic flow boiling in uniformly heated round tubes have been performed throughout the globe during the past sixty years for a variety of cryogens. However, the experimental data are scarce and either rarely published or published only for a few cryogens, with majority of the data remaining in the archives of authors, or in obscure technical reports of an organization or other inaccessible sources. In the present study, the Purdue University-Boiling and Two-Phase Flow Laboratory (PU-BTPFL) Cryogenic Total Pressure Drop Database is consolidated both for saturated adiabatic liquid-vapor and saturated flow boiling for cryogens from world literature dating back to 1964. With 474 total pressure drop data points for LHe, LH_2, LNe, and LN_2, it represents the largest total pressure drop database for cryogenic saturated two-phase flow assembled to date. Using this database, predictive accuracy of seminal frictional pressure gradient correlations employing both the Homogenous Equilibrium Model (HEM) and the Separated Flow Model (SFM) are assessed. The distinct fluid physics unique to cryogens is studied further using the database and new dimensionless criteria are developed to demarcate a dispersed flow dominant data subset from the separated flow dominant data subset, which are better represented using HEM and SFM, respectively. These criteria are subsequently used to develop a hybrid HEM-SEM frictional pressure gradient correlation for saturated cryogenic flow for the two distinct data subsets. The new hybrid correlation performs the best of all seminal correlations and provides excellent predictive agreement with the database, evidenced by a Mean Absolute Error (MAE) of 14.7 %.

1. Introduction

1.1. Applications of Cryogenic Fluids

Cryogenic fluids are used in a broad range of industries. For example, in the food industry, Liquid Nitrogen (LN_2) is used to fast freeze food, whereas in the healthcare industry, it is used to preserve tissues and blood, and to destroy unhealthy tissues in cryosurgery. Liquid Oxygen (LOX) is used in the healthcare industry especially in life support systems. Additionally, several cryogens, especially LOX, Liquid Hydrogen (LH_2), Liquid Methane (LCH_4), and Liquid Helium (LHe), have been used over the years in two primary applications: electronic cooling and space missions, the latter being the primary focus of the present study. In the field of electronic cooling, after an initial period of academic research interest in LHe heat transfer in West Germany [1], United States of America [2], and Japan [3,4] in the early 1970s, the decade of 1975–85 was a golden age for LHe flow boiling research in the Soviet Union in connection with development of forced convective cooling of superconducting systems [5–12]. Similar surge in LH_2 flow boiling research was observed in the decade post 2008 primarily in Japan, after a long gap with preliminary work done in the United States of America [13–15], with the objective of cooling large scale high temperature superconductor (HTS) magnets [16–25]. While LH_2 and LN_2 have been used over the years to cool high-temperature superconducting (HTS) magnets [16,26,27], LHe, having the lowest critical temperature of any known fluid, is also used to chill down Earth-orbiting telescopes and satellites as well as cool space experiments, where the ambient temperature in space is ~ 2.7 K. And, following some initial work around 1960, LCH_4, received renewed interest in 2010 at NASA's Glenn

* Corresponding author.
E-mail address: mudawar@purdue.edu (I. Mudawar).
[1] website: https://engineering.purdue.edu/BTPFL

https://doi.org/10.1016/j.ijheatmasstransfer.2023.124901
Received 4 August 2023; Received in revised form 18 October 2023; Accepted 31 October 2023
Available online 18 November 2023

Nomenclature

A	flow area
Bo	boiling number, q/Gh_{fg}
Bd	Bond number, $[g(\rho_f - \rho_g)D^2]/\sigma$
Ca_{fo}	liquid-only Capillary number, $\mu_f G/(\rho_f \sigma)$
C	coefficients in Separated Flow Model correlations in Table 4
D	tube's inner diameter
f_{sp}	Fanning friction factor corresponding to single-phase flow
f_{tp}	Fanning friction factor corresponding to two-phase flow
$Fr_{fo,D}$	liquid-only Froude number based on tube diameter, $G^2/[gD\rho_f^2]$
$Fr_{tp,D}$	two-phase homogeneous mixture Froude number based on tube diameter, $G^2/[gD\rho_{tp}^2]$
G	mass velocity
Ga	Galileo number, $[\rho_f g(\rho_f - \rho_g)D^3]/\mu_f^2$
g	gravitational acceleration
h	local enthalpy
h_f	enthalpy of saturated liquid
h_g	enthalpy of saturated vapor
h_{fg}	latent heat of vaporization, h_g - h_f
L_H	heated length of test section tube
L_{PH}	heated length of pre-heater section tube
L_{sp}	single-phase length, defined in Eqs. (11) and (12)
L_{tp}	two-phase length, defined in Eq. (10)
MAE	Mean Absolute Error, defined in Eq. (35)
P	pressure
ΔP_T	total pressure drop, defined in Eq. (18)
ΔP_{sp}	single-phase total pressure drop over the single-phase length, defined in Eq. (13)
$\Delta P_{sp,fo,F}$	hypothetical single-phase liquid frictional pressure drop over the two-phase length, assuming saturated liquid flow over the entire two-phase length
$\Delta P_{sp,go,F}$	hypothetical single-phase vapor frictional pressure drop over the two-phase length, assuming saturated vapor flow over the entire two-phase length
ΔP_{tp}	two-phase total pressure drop over the two-phase length, defined in Eq. (1)
$\Delta P_{tp,F}$	two-phase frictional pressure drop over the two-phase length
$\Delta P^*_{tp,F}$	dimensionless two-phase frictional pressure drop, $\frac{\Delta P_{tp,F} - \Delta P_{sp,fo,F}}{\Delta P_{sp,go,F} - \Delta P_{sp,fo,F}}$
P_{crit}	critical pressure
P_R	reduced pressure, P/P_{crit}
q	heat flux based on tube's inner heated surface area
$Re_{f,D}$	liquid Reynolds number based on tube diameter, $GD(1\text{-}x)/\mu_f$
$Re_{fo,D}$	liquid-only Reynolds number based on tube diameter, GD/μ_f
$Re_{g,D}$	vapor Reynolds number based on tube diameter, GDx/μ_g
$Re_{go,D}$	vapor-only Reynolds number based on tube diameter, GD/μ_g
$Re_{sp,D}$	single-phase Reynolds number based on tube diameter, defined in Eq. (16)
$Re_{tp,D}$	two-phase Reynolds number based on tube diameter, defined in Eq. (6)
RMS	Root Mean Squared error, defined in Eq. (36)
S	slip ratio, u_g/u_f
$Su_{fo,D}$	liquid-only Suratman number based on tube diameter, $\rho_f \sigma D/\mu_f^2$
$Su_{go,D}$	vapor-only Suratman number based on tube diameter, $\rho_g \sigma D/\mu_g^2$
T_λ	lambda point temperature (2.17 K) for liquid helium transitioning from LHe I to LHe II
u	mean fluid velocity
$u_{f,SFM}$	mean liquid velocity in a separated flow, defined in Eq. (28)
$u_{g,SFM}$	mean vapor velocity in a separated flow, defined in Eq. (29)
$u_{mix,HEM}$	two-phase mixture mean velocity in homogeneous dispersed flow, defined in Eq. (27)
$We_{fo,D}$	liquid-only Weber number based on tube diameter, $G^2D/(\rho_f \sigma)$
$We_{tp,D}$	two-phase homogeneous mixture Weber number based on tube diameter, $G^2D/(\rho_{tp}\sigma)$
x	flow quality
x_e	thermodynamic equilibrium quality, $(h - h_f)/h_{fg}$
$x_{e,in}$	inlet thermodynamic equilibrium quality based on pressure at inlet of heated length, $(h_{in} - h_{f,in})/h_{fg,in}$
$x_{e,out}$	outlet thermodynamic equilibrium quality determined from $x_{e,in}$, energy balance for entire heated length, and pressure at outlet of heated length, $(h_{out} - h_{f,out})/h_{fg,out}$
X	Lockhart-Martinelli parameter
z	axial coordinate along the tube
$\frac{\Delta z_{sat}}{L_H}$	saturation length ratio, $\frac{z - z_{x_e=0}}{L_H} = \frac{x_e}{4Bo}\left(\frac{D}{L_H}\right)$, defined by Ganesan *et al.* [34]
$\frac{\Delta z_{sat,tot.}}{L_H}$	total saturation length ratio, defined in Eq. (34)

Greek Symbol

α	void fraction
α_{HEM}	void fraction for HEM based formulation, defined in Eq. (22)
α_{SFM}	void fraction for SFM based formulation, defined in Eq. (24)
θ	percentage of data points predicted within ±30 %; tube's angle of inclination from horizontal
μ	dynamic viscosity
μ_{sp}	single-phase dynamic viscosity
μ_{tp}	two-phase homogeneous mixture dynamic viscosity in Table 3
υ	specific volume
ξ	percentage of data points predicted within ±50 %
ρ	density
ρ_{sp}	single-phase density
ρ_{tp}	two-phase homogeneous mixture density, $\rho_{tp} = \left[\frac{x}{\rho_g} + \frac{1-x}{\rho_f}\right]^{-1}$
σ	surface tension
ϕ	two-phase frictional pressure drop multiplier, defined in Eqs. (7) and (8)

Subscript

A	accelerational component
crit	critical point
exp	experimental (measured)
F	frictional component
f	saturated liquid
fo	liquid only
G	gravitational component
g	saturated vapor
go	vapor only
HEM	Homogenous Equilibrium Model
in	inlet
mix	two-phase homogeneous mixture
out	outlet
PH	pre-heater
pred	predicted

sat	saturated condition	T	total
SFM	Separated Flow Model	tp	two-phase
sp	single-phase (liquid or vapor)		

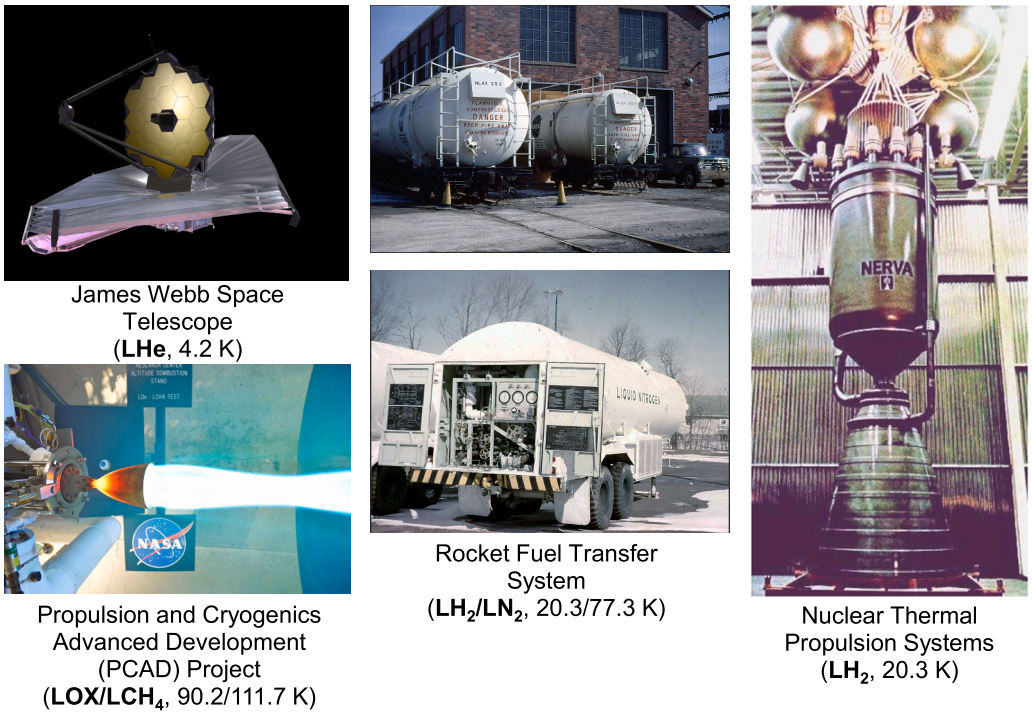

Fig. 1. Examples of space applications of cryogens.

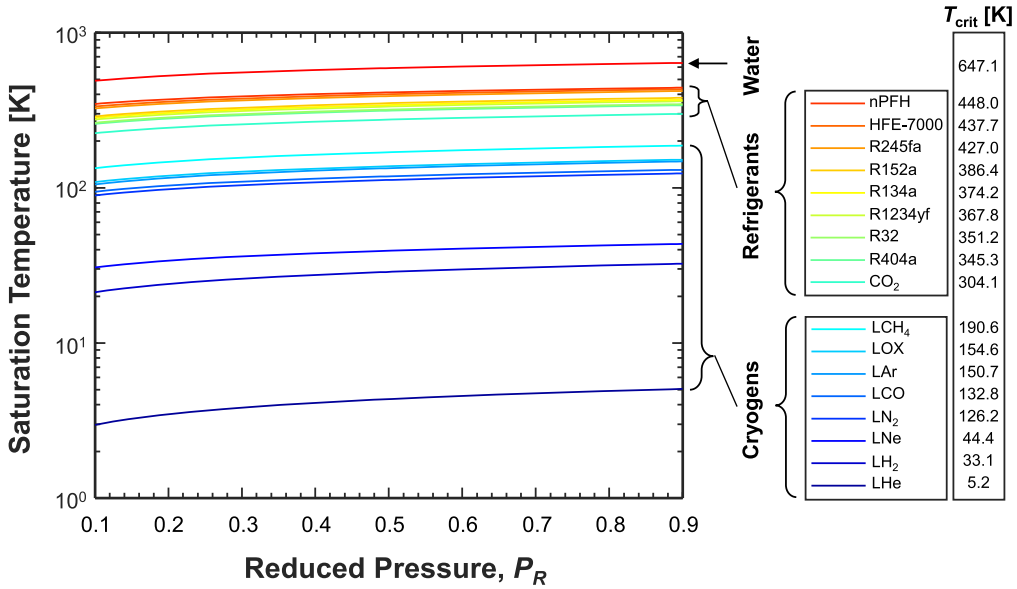

Fig. 2. Classification of coolants into water, refrigerants, and cryogens based on variation of saturation temperature with reduced pressure.

Research Center [28] and Johnson Space Center [29–31] as part of their Propulsion and Cryogenics Advanced Development (PCAD) project, where nontoxic propellants such as LOX/LCH_4 were being tested for spacecraft applications. In nuclear thermal propulsion systems, LOX/LCH_4 or LOX/LH_2 are used in ascent stages, descent stages, and in-space fuel depots. LH_2 has also been proposed for future use as both propellent and coolant in several other advanced propulsion systems. Fig. 1 shows examples of the space applications of cryogens.

Although almost all cryogens exist in unique states, LHe and LH_2 do not. LH_2 usually exists in two molecular spin states, orthohydrogen and parahydrogen, which exhibit significantly different thermal properties such as specific heat and thermal conductivity. Since the operating

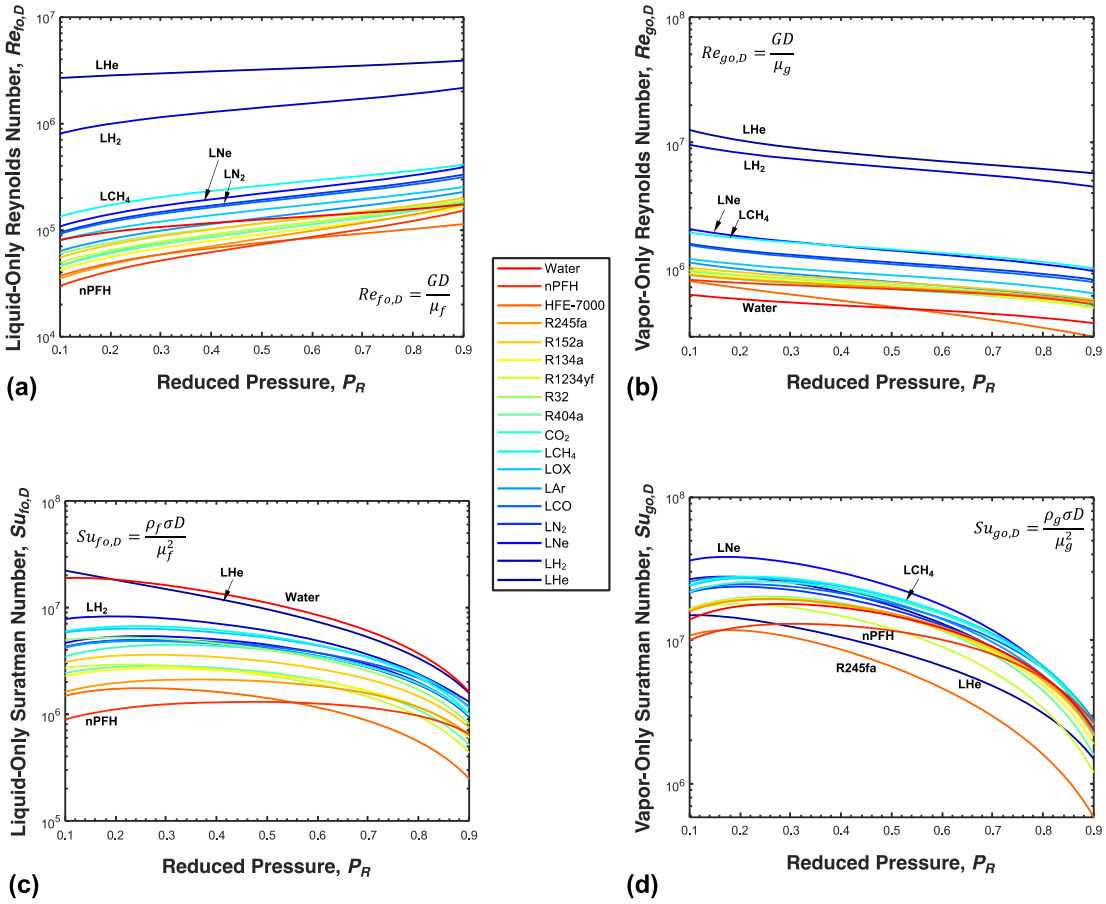

Fig. 3. Variations of (a) liquid-only Reynolds number, (b) vapor-only Reynolds number, (c) liquid-only Suratman number, and (d) vapor-only Suratman number with reduced pressure for cryogens along with those for other fluid classes under saturated conditions for a fixed mass velocity of $G = 1000$ kg/m^2.s and tube diameter of $D = 10$ mm.

temperature of LH_2 for applications of interest to the present study is ~ 20.4 K, it is predominantly parahydrogen (0.2 % ortho- and 99.8 % para-) as compared to orthohydrogen (75 % ortho- and 25 % para) at 300 K. Similarly, LHe exists in two states, LHe I (at temperatures greater than the lambda temperature, T_λ) and LHe II (at temperatures lower than T_λ). Since the operating temperature of LHe for space applications of interest is greater than 2.17 K, all the LHe data examined correspond to LHe I. From here on, liquid parahydrogen and liquid helium I will be referred to simply as LH_2 and LHe, respectively.

1.2. Fluid Physics Unique to Cryogens

Cryogens constitute a unique class of fluids which are clearly distinguishable from water and refrigerants by virtue of their low saturation temperatures, as shown in Fig. 2 (calculated using REFPROP 10 [32]). In addition to low saturation temperatures, cryogens also exhibit general thermophysical property trends, including (a) low surface tension, σ, (b) low latent heat of vaporization, h_{fg}, (c) low liquid viscosity, μ_f, (d) low vapor viscosity, μ_g, and, to a lesser extent, (e) low liquid-to-vapor density difference, ρ_f - ρ_g. Several consequences of this physics have been investigated by the current authors for mechanisms of critical heat flux (CHF) [33], saturated flow boiling heat transfer [34] and post-CHF saturated and superheated flow boiling heat transfer [35]. However, the consequences of unique thermophysical property trends of cryogens on the frictional pressure drop for saturated two-phase flows is better understood via magnitude of relevant dimensionless groups, which were identified by Kim and Mudawar [36] as prevalent in seminal frictional pressure gradient correlations. The trends for these dimensionless groups are captured in Fig. 3 and Fig. 4, for commonly used cryogens under saturated conditions by plotting against reduced pressures ranging from 0.1 to 0.9 for fixed mass velocity of $G = 1000$ kg/m^{2}s and tube diameter of $D = 10$ mm (macro-channel range).

Figs. 3(a)-(b) shows that by virtue of low liquid and vapor viscosities, cryogens in general exhibit higher liquid-only Reynolds number, $Re_{fo,D}$, as well as higher vapor-only Reynolds number, $Re_{go,D}$, as compared to water and refrigerants, with LHe and LH_2 having $Re_{fo,D}$ values at least one order of magnitude higher than the rest. Figs. 3(c)-(d) show variations of liquid-only Suratman number, $Su_{fo,D}$, and vapor-only Suratman number, $Su_{go,D}$. Unlike Reynolds number, which is the ratio of inertia to viscous force, Suratman number (also known as Laplace number) can be interpreted as the ratio of surface tension force to viscous force ($\sim Re^2/We$) and is used to characterize free-surface two-phase flows (e.g., annular flow). Fig. 3(c) shows that cryogens have higher $Su_{fo,D}$ values than most room temperature fluids (excepting water) and refrigerants, with LHe having the highest value among all cryogens. Fig. 3(d) shows that, despite most of the cryogens having higher $Su_{go,D}$ values than water and refrigerants, LHe shows an abnormally low magnitude while LNe has the highest value of all the fluids. Having the highest $Su_{fo,D}$ among all cryogens, as seen in Fig. 3(c), despite exhibiting low surface tension and low liquid and vapor viscosities, LHe shows greater dominance of stabilizing surface tension force on the annular free-surface as compared to the destabilizing viscous shear force on the liquid-film-side of the same annular free-surface. The opposite is true for the vapor-core-side of an annular free-surface of LHe, as seen in Fig. 3(d), where the destabilizing viscous shear force on the vapor-core-side on an annular free-surface shows relatively greater dominance as compared to the stabilizing

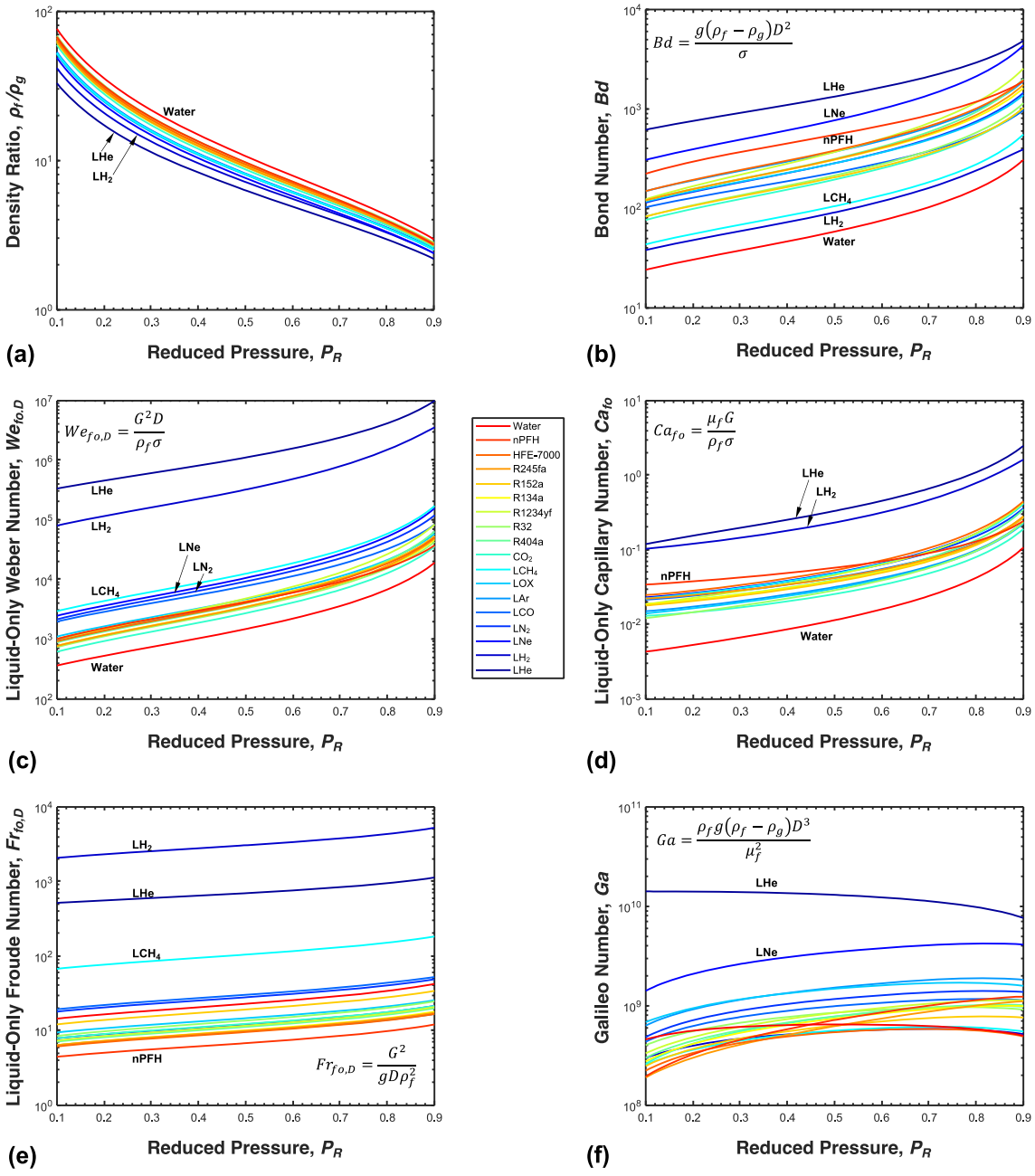

Fig. 4. Variations of (a) density ratio, (b) Bond number, (c) liquid-only Weber number, (d) liquid-only Capillary number, (e) liquid-only Froude number, and (f) Galileo number with reduced pressure for cryogens along with those for other fluid classes under saturated conditions for a fixed mass velocity of $G = 1000$ kg/m^2.s and tube diameter of $D = 10$ mm.

surface tension force on the same annular free-surface. These two inferences about LHe based on magnitudes of $Su_{fo,D}$ and $Su_{go,D}$ will later provide important insights into why LHe data are best predicted by the Homogeneous Equilibrium Model (HEM) (which is applicable mostly to dispersed flows, e.g., bubbly), as opposed to the Separated Flow Model (SFM) (which is applicable mostly to separated flows, e.g., annular) for flow qualities and void fractions spanning the entire spectrum from 0 to 1. The reasoning for such unique behavior for LHe can be explained as follows. By virtue of comparatively high $Su_{fo,D}$, the liquid-vapor free-surface interface in a LHe annular flow region would experience a relatively weaker destabilizing viscous shear force from the liquid continuum side of interface (*liquid film*), as opposed to the stabilizing surface tension force. However, due to comparatively low $Su_{go,D}$, the same liquid-vapor free-surface interface in a LHe annular flow region would experience a relatively stronger destabilizing viscous shear force from the vapor continuum side of interface (*vapor core*), as opposed to the stabilizing surface tension force. Due to steeper velocity gradient in the vapor core as compared to that in the liquid film as a consequence of higher vapor velocity due to lower vapor density, the viscous shear force from the vapor core side of interface is much higher than that from the liquid film side of the interface. Hence, the relatively stronger viscous shear force in the vapor core region would tend to distort and break the free-surface interface, causing significant *liquid entrainment* in the *vapor core* of the annular region. Therefore, a significant portion of the tube length would feature mostly dispersed flow dominant behavior be it bubbly flow or highly liquid droplets entrained annular flow. This inference would later be used to understand why the Homogenous Equilibrium Model works best for LHe even for separated flow dominant

Table 1
Operational ranges of controlled variables and corresponding dimensionless numbers for frictional pressure drop data points under saturated adiabatic (liquid-vapor) conditions in the present PU-BTPFL Cryogenic Pressure Drop Database and in database for mostly other common fluids.

Working Fluid(s)	Controlled Variables				Flow Characterizing Dimensionless Numbers		
	Reduced Pressure P_R	Tube Inner Diameter D x 10^3 [m]	Mass Velocity G [kg m^{-2} s^{-1}]	Flow Quality x	Liquid-Only Reynolds Number $Re_{fo,D}$ x 10^{-3}	Liquid Reynolds Number $Re_{f,D}$ x 10^{-3}	Vapor Reynolds Number $Re_{g,D}$ x 10^{-3}
LHe	0.29	2.13	31.96	0	36.7	0	0
	0.90	5.33	165.58	1	154.5	143.2	296.4
LNe	0.056	4	116	0.08	4.1	3	8.8
	0.056	4	120	0.25	4.2	3.9	26.5
LHe and LNe [a]	0.056 - 0.9	2.13 - 5.33	31.96 - 165.58	0 - 1	4.1 - 154.5	0 - 143.2	0 - 296.4
Air/CO_2/N_2–water mixtures, N_2–ethanol mixture, R12, R22, R134a, R236ea, R245fa, R404A, R410A, R407C, propane, CH_4, ammonia, CO_2, and water [b]	0.0052 - 0.91	0.0695 - 6.22	4 - 8528	0 - 1	3.9 x 10^{-3} - 89.79	0 - 79.2	0 - 253.8

[a] From 208 frictional pressure drop data points for saturated adiabatic liquid-vapor flow from current database with flow quality ranging from 0 to 1.
[b] From 7115 frictional pressure drop data points for saturated adiabatic liquid-vapor flow by Kim and Mudawar [36] with flow quality ranging from 0 to 1.

Table 2
Operational ranges of controlled variables and corresponding dimensionless numbers for frictional pressure drop data points under saturated boiling conditions in the present PU-BTPFL Cryogenic Pressure Drop Database and in database for mostly other common fluids.

Working Fluid(s)	Controlled Variables				Flow Characterizing Dimensionless Numbers		
	Reduced Pressure P_R	Tube Inner Diameter D x 10^3 [m]	Mass Velocity G [kg m^{-2} s^{-1}]	Flow Quality x	Liquid-Only Reynolds Number $Re_{fo,D}$ x 10^{-3}	Liquid Reynolds Number $Re_{f,D}$ x 10^{-3}	Vapor Reynolds Number $Re_{g,D}$ x 10^{-3}
LHe	0.49	2.13	41	0	36.7	0	0
	0.89	2.73	168	1	160.4	137	333.9
LH_2	0.14	4.77	532	0	379.4	13.4	0
	0.86	12.87	2735	1	2240.3	1794.9	6322.2
LNe	0.056	4	75.2	0.08	2.6	0.5	16.5
	0.056	4	140	0.82	4.9	3.6	85.7
LN_2	0.03	5.79	94.5	0	5	0	0
	0.05	11.73	300	1	16.1	11.51	370.2
LHe, LH_2, LNe, and LN_2 [a]	0.03 - 0.89	2.13 - 12.87	41 - 2735	0 - 1	2.6 - 2240.3	0 - 1794.9	0 - 6322.2
R12, R134a, R22, R245fa, R410A, FC-72, ammonia, CO_2, and water [b]	0.005 −0.78	0.349 - 5.35	33 - 2738	0 - 1	0.156 - 28.01	0 - 16.02	0 - 199.5

[a] From 266 frictional pressure drop data points for saturated two-phase flow boiling from current database with flow quality ranging from 0 to 1.
[b] From 2378 frictional pressure drop data points for saturated two-phase flow boiling by Kim and Mudawar [37] with flow quality ranging from 0 to 1.

data. Another unique trait is observed in Fig. 3(d) for LNe based on having the highest value of $Su_{go,D}$ among all fluids including cryogens. Hence, LNe exhibits stronger stabilizing surface tension force on the annular free-surface as compared to the destabilizing viscous shear force on the vapor-core-side of the same annular free-surface. Hence, the relatively stronger surface tension force in the vapor core region would tend to keep the free-surface interface in the annular flow region stable *without* causing any liquid entrainment in the vapor core of the annular region. Therefore, for LNe, a stable separated, annular flow regime will be established downstream which would later be identified to work best with the Separated Flow Model.

Fig. 4(a) shows that cryogens in general possess a lower density ratio, ρ_f/ρ_g, as opposed to water and refrigerants, with LHe having the lowest ratio among cryogens. The consequence of density difference, ρ_f - ρ_g, trends for cryogens is captured in variations of the Bond number, *Bd*, with reduced pressure, Fig. 4(b). Since *Bd* is the ratio of buoyancy force to surface tension force, which both generally have low values for cryogens, the corresponding *Bd* trends are not straightforward. It is seen that, while LHe and LNe exhibit relatively high values of *Bd*, LH_2 and LCH_4 show comparatively low values. Fig. 4(c)-(d) show both LHe and LH_2 also exhibit higher values of liquid-only Weber number, $We_{fo,D}$, and liquid-only Capillary number, Ca_{fo} ($\sim We_{fo,D}/Re_{fo,D}$). This is indicative of comparatively weaker surface tension for LHe and LH_2 compared to other cryogens. However, this trend is not reflected in the same manner for LHe by $Su_{fo,D}$, in Fig. 3(c), which is applicable to free-surface liquid-vapor interface observed in annular flow regime. To better understand the trends of $Su_{fo,D}$ and $We_{fo,D}$, it is important to point out the difference in the applicability of inferences derived from the trends of Suratman number and Weber number. While Suratman (or Laplace) number is applicable to free-surface liquid-vapor interface, viz. annular flow, Weber number is applicable to strongly curved interfaces, viz. vapor bubbles. Thus, for LHe, high values of *Bd*, $We_{fo,D}$, and Ca_{fo} are indicative of stronger buoyancy force, liquid inertia force, and liquid viscous shear force on the vapor bubbles as compared to the surface tension force in the dispersed bubbly flow regime. Hence, the liquid-vapor curved interface for LHe would tend to get unstable and break into smaller bubbles if one of three aforementioned forces act on it. This further explains the nature of bubble and flow features for LHe which tends to

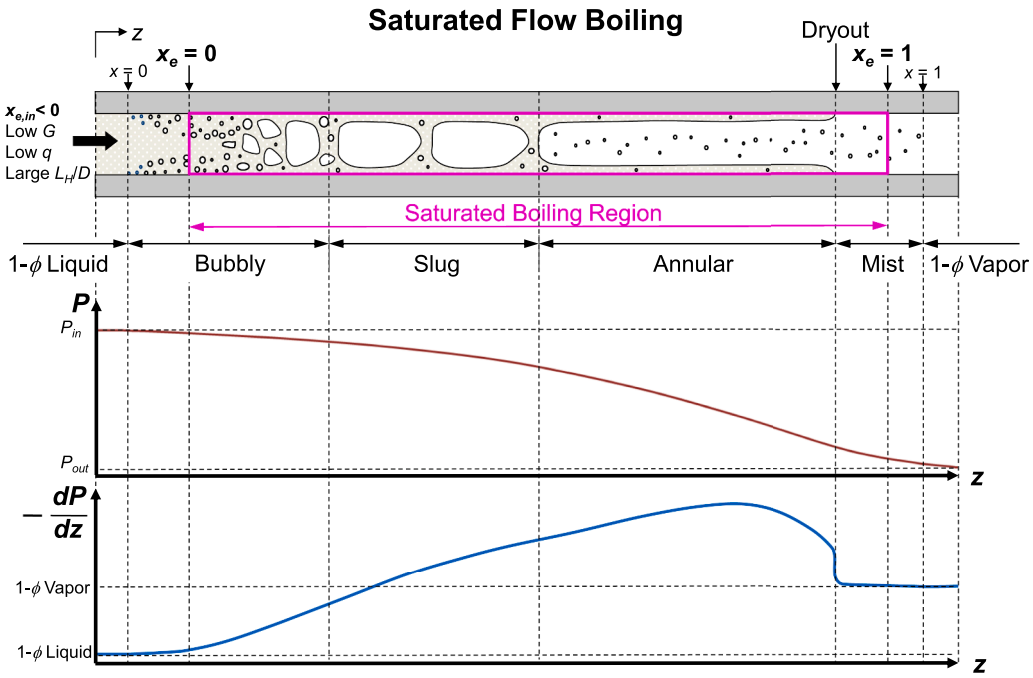

Fig. 5. Schematic of flow regimes and variations of pressure and pressure gradient along a uniformly heated tube with subcooled inlet conditions ($x_{e,in} < 0$) and superheated outlet conditions ($x_{e,out} > 1$).

be dispersed flow dominant whose frictional pressure gradient is seen to be best captured using Homogenous Equilibrium Model which are best applicable to dispersed flows. Hence, despite LHe vapor bubbles coalescing to form large oblong vapor bubbles, the relatively stronger destabilizing liquid inertial force and liquid viscous shear force in the liquid continuum region as opposed to stabilizing surface tension force would tend to distort and break the strongly curved bubble interface, reducing the large vapor bubbles to smaller vapor bubbles, by virtue of high values of $We_{fo,D}$ and Ca_{fo}. Hence, throughout the tube, LHe flow features tend to be dispersed flow dominant, be it in the bubbly flow region (due to high $We_{fo,D}$ and Ca_{fo}) or in the annular flow region with high liquid droplet entrainment in the vapor core (due to low $Su_{go,D}$). This behavior is truly unique to LHe. Fig. 4(e) shows that cryogens generally exhibit higher liquid-only Froude number ($Fr_{fo,D}$) values, especially LH_2, LHe and LCH_4, than water and refrigerants, which implies stronger inertia compared to gravity. Finally, Fig. 4(f) shows that LHe and LNe have the highest values of Galileo number, *Ga*, with implies they are associated with higher ratio of buoyancy to viscous force compared to other fluids. Figs. 4(e) and (f) combined show relative importance of inertia, viscous force, and gravity for the different cryogens.

Given the trends presented thus far, it is evident that (i) cryogens behave differently from water and refrigerants, and (ii) even among cryogens, LHe and LNe act as outliers. These facts suggest that owing to unique fluid physics of cryogens, pressure drop and heat transfer correlation studies are best pursued separately from those of other fluid classes, with LHe and LNe requiring special treatment among the cryogens.

In addition to the fluid physics unique to cryogens, there are several experimental issues unique to cryogens, especially temperature measurement uncertainties, heated tube material axial conduction effects, and extreme (supercritical) wall and vapor temperatures attainable post-CHF. These have been addressed extensively in previous studies by the current authors [33–35] as part of their investigation of cryogenic flow boiling spanning the entire boiling curve.

To achieve the goal of developing frictional pressure gradient correlations for saturated two-phase flow for cryogens, data are amassed from the literature and consolidated into a new Purdue University-Boiling and Two-Phase Flow Laboratory (PU-BTPFL) Cryogenic Two-Phase Flow Total Pressure Drop Database (PU-BTPFL Cryogenic Pressure Drop Database for short), which will be discussed in subsequent sections, the largest ever assembled for cryogens. Table 1 provides details of ranges of saturated adiabatic two-phase flow data within the present consolidated database, including controlled variables (P_R, *D*, *G*, and *x*) and associated flow characterizing dimensionless numbers ($Re_{fo,D}$, $Re_{f,D}$, and $Re_{g,D}$), alongside the largest adiabatic two-phase pressure drop database for mostly other fluid classes from Kim and Mudawar [36]. Table 2 provides similar details for saturated flow boiling data within the present consolidated database and that of Kim and Mudawar [37]. These two tables show that despite the low data count for cryogens, the operational range span is comparable to the ones generated by Kim and Mudawar [36,37] for other fluid classes, which further speaks to the broad applicability of the present consolidated database for analysis of pressure drop for cryogens.

1.3. Objectives of Present Study

The present study is motivated by (i) the lack of a unified, comprehensive, and reliable total pressure drop (ΔP_T) database for both adiabatic (liquid-vapor) saturated two-phase flow and saturated flow boiling of cryogens in a uniformly heated tube, and (ii) the lack of an accurate correlation universally valid for different cryogens. Following are key objectives of the study:

(1) Amass from the world literature cryogenic saturated flow ΔP_T data (both for adiabatic liquid-vapor and for saturated two-phase flow boiling) for cryogens in uniformly heated tubes.
(2) Using systematic criteria, assess the accumulated data on a point-by-point basis to exclude any that are inaccurate or missing vital information such as operating conditions.
(3) Compile the data into a new consolidated database Purdue University-Boiling and Two-Phase Flow Laboratory (PU-BTPFL) Cryogenic Total Pressure Drop Database (PU-BTPFL Cryogenic Pressure Drop Database for short) after applying the exclusion criteria.

Table 3
Two-phase mixture viscosity models employed in the Homogenous Equilibrium Model (HEM).

Author(s)	Equation
McAdams *et al.* [38]	$\frac{1}{\mu_{tp}} = \frac{x}{\mu_g} + \frac{1-x}{\mu_f}$
Akers *et al.* [39]	$\mu_{tp} = \frac{\mu_f}{\left[(1-x) + x\left(\frac{v_g}{v_f}\right)^{0.5}\right]}$
Cicchitti *et al.* [40]	$\mu_{tp} = x\mu_g + (1-x)\mu_f$
Owens [41]	$\mu_{tp} = \mu_f$
Dukler *et al.* [42]	$\mu_{tp} = \frac{xv_g\mu_g + (1-x)v_f\mu_f}{xv_g + (1-x)v_f}$
Lin *et al.* [43]	$\mu_{tp} = \frac{\mu_f\mu_g}{\mu_g + x^{1.4}(\mu_f - \mu_g)}$
Beattie and Whalley [44]	$\mu_{tp} = \omega\mu_g + (1-\omega)(1+2.5\omega)\mu_f$ $\omega = \frac{xv_g}{v_f + xv_{fg}}$

(4) Carefully segregate the data based on fluid (LHe, LH_2, LNe, LN_2, LCH_4), flow orientation (vertical upflow, vertical downflow, horizontal flow), inlet fluid state (subcooled liquid, saturated liquid, two-phase mixture), two-phase flow distribution (turbulent liquid-turbulent vapor, turbulent liquid-laminar vapor, laminar liquid-turbulent vapor), dominant two-phase flow regime (dispersed flow, separated flow), and tube material.
(5) Identify new physics-based classifiers that aid in understanding of physics unique to cryogens prior to correlation development.
(6) Apply the new physics-based classifiers to segregate dispersed flow cryogenic total pressure drop data from separated flow data.
(7) Assess the performance of prior seminal two-phase frictional pressure gradient correlations using the PU-BTPFL Cryogenic Pressure Drop Database.
(8) Using the PU-BTPFL Cryogenic Pressure Drop Database, develop new *universal* two-phase frictional pressure gradient correlations for cryogenic saturated two-phase flow.
(9) Identify *gaps* in the available data which warrant further experimental investigation.
(10) Recommend a methodology for acquiring future ΔP_T data in a manner that is conducive to refining two-phase frictional pressure gradient correlations and/or mechanistic models.

2. Pressure Drop Calculation Methods

2.1. Two-Phase Pressure Drop Components

In two-phase flow experiments, the total pressure drop across the ends of the tube is dictated by (i) heating conditions (adiabatic versus diabatic/boiling), (ii) flow orientation, and (iii) flow regime development along the tube. Based on the experimentally controlled variables of G, q, $x_{e,in}$, heated length, L_H, and inlet pressure, P_{in}, a range of flow regimes can be achieved, culminating in a region where saturated flow boiling will occur. The exhaustive set of possible flow regimes for all possible permutations of operating conditions that culminate in a saturated flow boiling region in a uniformly heated tube were discussed in detail in Ganesan *et al.* [34]. One such possible permutation is shown in Fig. 5, where both bubbly flow and annular flow are observed in the saturated boiling region. Notice that with a subcooled inlet ($x_{e,in} < 0$), the saturated boiling region extends from $x_e = 0$ to $x_e = 1$ beyond the location of Dryout-type CHF for low G, low q, and large L_H/D. This particular permutation is one that includes all possible flow regimes within the saturated boiling region from bubbly to slug to annular to mist. Fig. 5 also shows the variations of pressure and pressure gradient along the tube.

To better understand those variations, the two-phase total pressure drop within the saturated region ($0 \le x_e \le 1$) can be expressed as the sum of frictional, gravitational, and accelerational components,

$$\Delta P_{tp} = \Delta P_{tp,F} + \Delta P_{tp,G} + \Delta P_{tp,A} \tag{1}$$

The two-phase acclerational pressure gradient can be expressed as

$$-\left(\frac{dP}{dz}\right)_{tp,A} = G^2\frac{d}{dz}\left[\frac{v_g x^2}{\alpha} + \frac{v_f(1-x)^2}{(1-\alpha)}\right] \tag{2}$$

where x and α are values of local flow quality and local void fraction. And the two-phase gravitational pressure gradient can be expressed as

$$-\left(\frac{dP}{dz}\right)_{tp,G} = \left[\alpha\rho_g + (1-\alpha)\rho_f\right] g\sin\theta \tag{3}$$

where θ is the tube's angle of inclination from horizontal.

For the special case of adiabatic two-phase flow, the two-phase accelerational pressure gradient, $-(dP/dz)_{tp,A}$, can be approximated to zero because of negligible property variations with pressure. Additionally, for horizontal flow orientation ($\theta = 0$), the two-phase gravitational pressure gradient, $-(dP/dz)_{tp,G}$, is equal to zero. Hence, for adiabatic horizontal two-phase flow, the two-phase total pressure drop would equal the frictional pressure drop ($\Delta P_{tp} = \Delta P_{tp,F}$).

The two-phase frictional pressure gradient, $-(dP/dz)_{tp,F}$, can be predicted according to either the Homogeneous Equilibrium Model (HEM) or semi-empirical Separated Flow Model (SFM) correlations. HEM treats the two-phase mixture as a pseudo-fluid possessing properties that are dictated by local flow quality. Further, HEM assumes that both the liquid and vapor are moving with the same velocity ($u_f = u_g = u_{mix,HEM}$). The SFM formulation on the other hand allows separate treatments of the liquid and vapor flows by allowing different phase velocities ($u_{f,SFM} \neq u_{g,SFM}$). Hence, using HEM to predict the two-phase frictional pressure gradient is more appropriate for dispersed flow regimes (bubbly flow pre-CHF and mist flow post-CHF), whereas SFM is more appropriate for separated flow regimes (annular flow pre-CHF and inverted annular flow post-CHF).

With HEM, the two-phase frictional pressure gradient can be determined from

$$-\left(\frac{dP}{dz}\right)_{tp,F} = \frac{2f_{tp}G^2}{\rho_{tp}D} = \frac{2f_{tp}G^2}{D}\left(\frac{x}{\rho_g} + \frac{1-x}{\rho_f}\right) \tag{4}$$

where

$$f_{tp} = 16Re_{tp,D}^{-1} \text{ for } Re_{tp,D} < 2000 \tag{5a}$$

$$f_{tp} = 0.079Re_{tp,D}^{-0.25} \text{ for } 2000 \le Re_{tp,D} < 20,000 \tag{5b}$$

and

$$f_{tp} = 0.046Re_{tp,D}^{-0.2} \text{ for } Re_{tp,D} \ge 20,000 \tag{5c}$$

Table 3 provides several two-phase mixture viscosity (μ_{tp}) relations that are used to calculate the two-phase Reynolds number, $Re_{tp,D}$, which is defined as

$$Re_{tp,D} = \frac{GD}{\mu_{tp}} \tag{6}$$

Table 4 shows a summary of seminal semi-empirical SFM-based formulations for determining the two-phase frictional pressure gradient. Although a more comprehensive list of SFM correlations is provided in Kim and Mudawar [48], only those correlations that exclude micro-channels are provided in Table 4 considering their applicability to the data points in the PU-BTPFL Cryogenic Pressure Drop database with $2.13 \le D$ (mm) ≤ 12.88. In the SFM formulation, the two-phase frictional pressure gradient can be determined using either Eqs. (7) or (8).

Table 4
Summary of seminal semi-empirical Separated Flow Model (SFM) formulations for two-phase frictional pressure gradient.

Author(s)	Equation(s)	Semi-Empirical Formulation	
Lockhart & Martinelli [a,c] [45]	$-\left(\frac{dP}{dz}\right)_{tp,F} = -\left(\frac{dP}{dz}\right)_{sp,f,F}\phi_f^2$		C
	where $\phi_f^2 = 1+\frac{C}{X}+\frac{1}{X^2}$, $X^2 = \frac{-\left(\frac{dP}{dz}\right)_{sp,f,F}}{-\left(\frac{dP}{dz}\right)_{sp,g,F}}$	$Re_{f,D} \geq 2000$, $Re_{g,D} \geq 2000$ (tt)	20
		$Re_{f,D} \geq 2000$, $Re_{g,D} < 2000$, (tv)	10
		$Re_{f,D} < 2000$, $Re_{g,D} \geq 2000$ (vt)	12
	$-\left(\frac{dP}{dz}\right)_{sp,f,F} = \frac{2f_{sp,f}G^2(1-x)^2}{\rho_f D}$, $-\left(\frac{dP}{dz}\right)_{sp,g,F} = \frac{2f_{sp,g}G^2x^2}{\rho_g D}$	$Re_{f,D} < 2000$, $Re_{g,D} < 2000$, (vv)	5
	$f_{sp,k} = 16Re_{k,D}^{-1}$ for $Re_{k,D} < 2000$		
	$f_{sp,k} = 0.079Re_{k,D}^{-0.25}$ for $2000 \leq Re_{k,D} < 20,000$		
	$f_{sp,k} = 0.046Re_{k,D}^{-0.2}$ for $Re_{k,D} \geq 20,000$		
	$Re_{f,D} = \frac{GD(1-x)}{\mu_f}$, $Re_{g,D} = \frac{GDx}{\mu_g}$		
	where subscript k denotes f or g for liquid and vapor phases, respectively		
Friedel [a,c] [46]	$-\left(\frac{dP}{dz}\right)_{tp,F} = -\left(\frac{dP}{dz}\right)_{sp,fo,F}\phi_{fo}^2$	$\phi_{fo}^2 = (1-x^2)+x^2\left(\frac{\rho_f}{\rho_g}\right)\left(\frac{f_{sp,go}}{f_{sp,fo}}\right)+$	
	where	$3.24x^{0.78}(1-x)^{0.224}\left(\frac{\rho_f}{\rho_g}\right)^{0.91}\left(\frac{\mu_g}{\mu_f}\right)^{0.19}\left(1-\frac{\mu_g}{\mu_f}\right)^{0.7}Fr_{tp,D}^{-0.045}We_{tp,D}^{-0.035}$	
	$-\left(\frac{dP}{dz}\right)_{sp,fo,F} = \frac{2f_{sp,fo}G^2}{\rho_f D}$		
	$f_{sp,ko} = 16Re_{ko,D}^{-1}$ for $Re_{ko,D} < 2000$		
	$f_{sp,ko} = 0.079Re_{ko,D}^{-0.25}$ for $2000 \leq Re_{ko,D} < 20,000$		
	$f_{sp,ko} = 0.046Re_{ko,D}^{-0.2}$ for $Re_{ko,D} \geq 20,000$		
	$Fr_{tp,D} = \frac{G^2}{gD\rho_{tp}}$, $We_{tp,D} = \frac{G^2D}{\rho_{tp}\sigma}$, $\frac{1}{\rho_{tp}} = \frac{x}{\rho_g}+\frac{1-x}{\rho_f}$		
	$Re_{fo,D} = \frac{GD}{\mu_f}$, $Re_{go,D} = \frac{GD}{\mu_g}$		
	where subscript ko denotes fo or go for liquid and vapor phases, respectively		
Müller-Steinhagen & Heck [a,c] [47]	$-\left(\frac{dP}{dz}\right)_{tp,F} = -\left(\frac{dP}{dz}\right)_{sp,fo,F}\phi_{fo}^2$	$\phi_{fo}^2 = \left\{1+2\left[\left(\frac{f_{sp,go}}{f_{sp,fo}}\right)\left(\frac{\rho_f}{\rho_g}\right)-1\right]x\right\}(1-x)^{1/3}+\left(\frac{f_{sp,go}}{f_{sp,fo}}\right)\left(\frac{\rho_f}{\rho_g}\right)x^3$	
	where		
	$-\left(\frac{dP}{dz}\right)_{sp,fo,F} = \frac{2f_{sp,fo}G^2}{\rho_f D}$, $-\left(\frac{dP}{dz}\right)_{sp,go,F} = \frac{2f_{sp,go}G^2}{\rho_g D}$		
	$f_{sp,ko} = 16Re_{ko,D}^{-1}$ for $Re_{ko,D} < 2000$		
	$f_{sp,ko} = 0.079Re_{ko,D}^{-0.25}$ for $2000 \leq Re_{ko,D} < 20,000$		
	$f_{sp,ko} = 0.046Re_{ko,D}^{-0.2}$ for $Re_{ko,D} \geq 20,000$		
	$Re_{fo,D} = \frac{GD}{\mu_f}$, $Re_{go,D} = \frac{GD}{\mu_g}$		
	where subscript ko denotes fo or go for liquid and vapor phases, respectively.		
Kim & Mudawar [b,d] [37]	$-\left(\frac{dP}{dz}\right)_{tp,F} = -\left(\frac{dP}{dz}\right)_{sp,f,F}\phi_f^2$		$C_{adiabatic}$
	where $\phi_f^2 = 1+\frac{C}{X}+\frac{1}{X^2}$, $X^2 = \frac{-\left(\frac{dP}{dz}\right)_{sp,f,F}}{-\left(\frac{dP}{dz}\right)_{sp,g,F}}$	$Re_{f,D} \geq 2000$, $Re_{g,D} \geq 2000$ (tt)	$0.386Re_{fo,D}^{0.03}Su_{go,D}^{0.10}\left(\frac{\rho_f}{\rho_g}\right)^{0.35}$
		$Re_{f,D} \geq 2000$, $Re_{g,D} < 2000$ (tv)	$8.7\times10^{-4}Re_{fo,D}^{0.17}Su_{go,D}^{0.50}\left(\frac{\rho_f}{\rho_g}\right)^{0.14}$
		$Re_{f,D} < 2000$, $Re_{g,D} \geq 2000$ (vt)	$0.0015Re_{fo,D}^{0.59}Su_{go,D}^{0.19}\left(\frac{\rho_f}{\rho_g}\right)^{0.36}$
	$-\left(\frac{dP}{dz}\right)_{sp,f,F} = \frac{2f_{sp,f}G^2(1-x)^2}{\rho_f D}$ $-\left(\frac{dP}{dz}\right)_{sp,g,F} = \frac{2f_{sp,g}G^2x^2}{\rho_g D}$, $f_{sp,k} = 16Re_{k,D}^{-1}$ for $Re_{k,D} <$ 2000	$Re_{f,D} < 2000$, $Re_{g,D} < 2000$ (vv)	$3.5\times10^{-5}Re_{fo,D}^{0.44}Su_{go,D}^{0.50}\left(\frac{\rho_f}{\rho_g}\right)^{0.48}$
	$f_{sp,k} = 0.079Re_{k,D}^{-0.25}$ for $2000 \leq Re_{k,D} < 20,000$		
	$f_{sp,k} = 0.046Re_{k,D}^{-0.2}$ for $Re_{k,D} \geq 20,000$		
	$Re_{fo,D} = \frac{GD}{\mu_f}$, $Su_{go,D} = \frac{\rho_g\sigma D}{\mu_g^2}$, $We_{fo,D} = \frac{G^2D}{\rho_f\sigma}$, $Bo = \frac{q}{Gh_{fg}}$		
	$Re_{f,D} = \frac{GD(1-x)}{\mu_f}$, $Re_{g,D} = \frac{GDx}{\mu_g}$		
	where subscript k denotes f or g for liquid and vapor phases, respectively	for $Re_{f,D} \geq 2000$	$C = C_{adiabatic}[1+60We_{fo,D}^{0.32}Bo^{0.78}]$
		for $Re_{f,D} < 2000$	$C = C_{adiabatic}[1+530We_{fo,D}^{0.52}Bo^{1.09}]$

[a] Applicable to only saturated adiabatic liquid-vapor two-phase flows.
[b] Applicable to both saturated adiabatic liquid-vapor and saturated flow boiling two-phase flows.
[c] Recommended for macro-channel two-phase flows.
[d] Recommended for mini- and micro-channel two-phase flows.

$$-\left(\frac{dP}{dz}\right)_{tp,F} = -\left(\frac{dP}{dz}\right)_{sp,f,F}\phi_f^2 \tag{7}$$

$$-\left(\frac{dP}{dz}\right)_{tp,F} = -\left(\frac{dP}{dz}\right)_{sp,fo,F}\phi_{fo}^2 \tag{8}$$

Eqs. (7) and (8) express the two-phase frictional pressure gradient as the product of the frictional pressure gradient for liquid phase and a corresponding two-phase frictional pressure drop multiplier. While in Eq. (7), the frictional pressure gradient for the liquid phase is based on the actual liquid flow rate, in Eq. (8) the frictional pressure gradient for

the liquid phase is based on the total flow rate. While Lockhart and Martinelli [45] and Kim and Mudawar [37] follow the functional form of Eq. (7), Friedel [46] and Müller-Steinhagen and Heck [47] follow Eq. (8). Detailed relations to find both the frictional pressure gradient for liquid phase and the corresponding two-phase multipliers are given in Table 4.

The two-phase pressure drop, ΔP_{tp}, is determined by numerically integrating the sum of frictional, gravitational, and accelerational pressure gradient components over the saturated boiling length, also referred to as the two-phase length, L_{tp}.

$$\Delta P_{tp} = \int_0^{L_{tp}} \left[-\left(\frac{dP}{dz}\right)_{tp,F} - \left(\frac{dP}{dz}\right)_{tp,G} - \left(\frac{dP}{dz}\right)_{tp,A} \right] dz \tag{9}$$

Since this study is focused on saturated two-phase flow, L_{tp} is defined as the distance between the locations where the thermodynamic equilibrium quality, x_e, is equal to 0 and 1. Thus, the two-phase length, L_{tp}, is defined as

$$L_{tp} = z_{x_e=1} - z_{x_e=0} \tag{10}$$

where x_e at any z location can be found using a simple energy balance.

2.2. Single-Phase Pressure Drop Components

In the current study, the region of non-equilibrium before the saturated boiling length, $z_{x_e=0} - z_{x=0}$, is not considered in two-phase pressure drop calculations and this region is merged with the single-phase liquid region. Similarly, the region of non-equilibrium after the saturated boiling length, $z_{x=1} - z_{x_e=1}$, is not considered in the two-phase drop calculations and this region is merged with the single-phase vapor region. Hence, the single-phase liquid length, $L_{sp,f}$, and the single-phase vapor length, $L_{sp,g}$, are defined, respectively, as

$$L_{sp,f} = z_{x_e=0} - z_{x_e=\min\{x_{e,in},0\}} \tag{11}$$

$$L_{sp,g} = z_{x_e=\max\{x_{e,out},1\}} - z_{x_e=1} \tag{12}$$

In either of the single-phase regions, the single-phase pressure drop, ΔP_{sp}, is determined by numerically integrating the sum of frictional and gravitational pressure gradient components over the corresponding single-phase length, L_{sp},

$$\Delta P_{sp} = \int_0^{L_{sp}} \left[-\left(\frac{dP}{dz}\right)_{sp,F} - \left(\frac{dP}{dz}\right)_{sp,G} \right] dz \tag{13}$$

where the single-phase frictional pressure gradient can be expressed as

$$-\left(\frac{dP}{dz}\right)_{sp,F} = \frac{2f_{sp}G^2}{\rho_{sp}D} \tag{14}$$

where

$$f_{sp} = 16Re_{sp,D}^{-1} \text{ for } Re_{sp,D} < 2000 \tag{15a}$$

$$f_{sp} = 0.079Re_{sp,D}^{-0.25} \text{ for } 2000 \le Re_{sp,D} < 20,000 \tag{15b}$$

and

$$f_{sp} = 0.046Re_{sp,D}^{-0.2} \text{ for } Re_{sp,D} \ge 20,000 \tag{15c}$$

In Eq. (15a)-(15c), the single-phase Reynolds number is found by evaluating the single-phase viscosity at the local pressure and bulk temperature, with the latter found using energy balance.

$$Re_{sp,D} = \frac{GD}{\mu_{sp}} \tag{16}$$

The single-phase gravitational pressure gradient can be expressed as

$$-\left(\frac{dP}{dz}\right)_{sp,G} = \rho_{sp} g \sin\theta \tag{17}$$

where the single-phase density is also evaluated at the local pressure and bulk temperature.

2.3. Determination of Measured Two-Phase Frictional Pressure Drop from Measured Total Pressure Drop

The total pressure-drop, ΔP_T, in a straight heated or unheated tube can be expressed as

$$\Delta P_T = \Delta P_{sp,f} + \Delta P_{tp} + \Delta P_{sp,g} \tag{18}$$

where the single-phase pressure drop components can be zero or non-zero depending on the inlet quality and exit quality conditions in accordance with Eqs. (11) and (12). Thus, for a given experimental total pressure drop, $\Delta P_{T,exp}$, across a straight heated or unheated tube, the experimental two-phase total pressure drop, $\Delta P_{tp,exp}$, is given by

$$\Delta P_{tp,exp} = \Delta P_{T,exp} - \Delta P_{sp,f} - \Delta P_{sp,g} \tag{19}$$

and the experimental two-phase frictional pressure drop, $\Delta P_{tp,F,exp}$, can be expressed as

$$\Delta P_{tp,F,exp} = \Delta P_{T,exp} - \Delta P_{sp,f} - \Delta P_{sp,g} - \Delta P_{tp,G} - \Delta P_{tp,A} \tag{20}$$

where, $\Delta P_{tp,F,exp}$ would vary depending on the relation for void fraction, α, used to calculate the accelerational ($\Delta P_{tp,A}$) and gravitational ($\Delta P_{tp,G}$) pressure drop components. This will be discussed in the next section.

From the above analysis, the axial variation of pressure and pressure gradient along a heated tube incurring saturated two-phase flow boiling, as shown in Fig. 5, can now be better understood. Due to the hydraulic resistances offered in the single-phase liquid, two-phase, and single-phase vapor regions, the local pressure decreases monotonically from P_{in} at the inlet to P_{out} at the outlet. Additionally, the pressure drop gradient is shallowest in the single-phase liquid region, steeper in the single-phase vapor region and steepest in the two-phase region, especially in the annular flow region where separated flow exists. The pressure drop gradients in the single-phase liquid and single-phase vapor regions are only due to the frictional components, but the vapor region has a steeper frictional pressure gradient due to its lower density that increases the vapor velocity from mass conservation. The pressure gradient in the two-phase region is due to both the frictional and accelerational components, with the latter resulting from the phase change occurring between the liquid and vapor adding momentum to the flow.

2.4. Void Fraction Relations

The choice of relation for void fraction, α, plays an important role is determining the two-phase accelerational and gravitational pressure gradients as seen in Eqs. (2) and (3). In general, void fraction can be expressed in terms of flow quality, x, density ratio, ρ_g/ρ_f, and slip ratio, $S = u_g/u_f$.

$$\alpha = \left[1 + \left(\frac{1-x}{x}\right)\left(\frac{\rho_g}{\rho_f}\right) S \right]^{-1} \tag{21}$$

Since, HEM assumes a slip ratio of unity, or $u_g = u_f$, Eq. (21) can be simplified for HEM as

$$\alpha_{HEM} = \left[1 + \left(\frac{1-x}{x}\right)\left(\frac{\rho_g}{\rho_f}\right) \right]^{-1} \tag{22}$$

It is recommended to use Eq. (22) when finding the two-phase accelerational and gravitational pressure gradients when employing

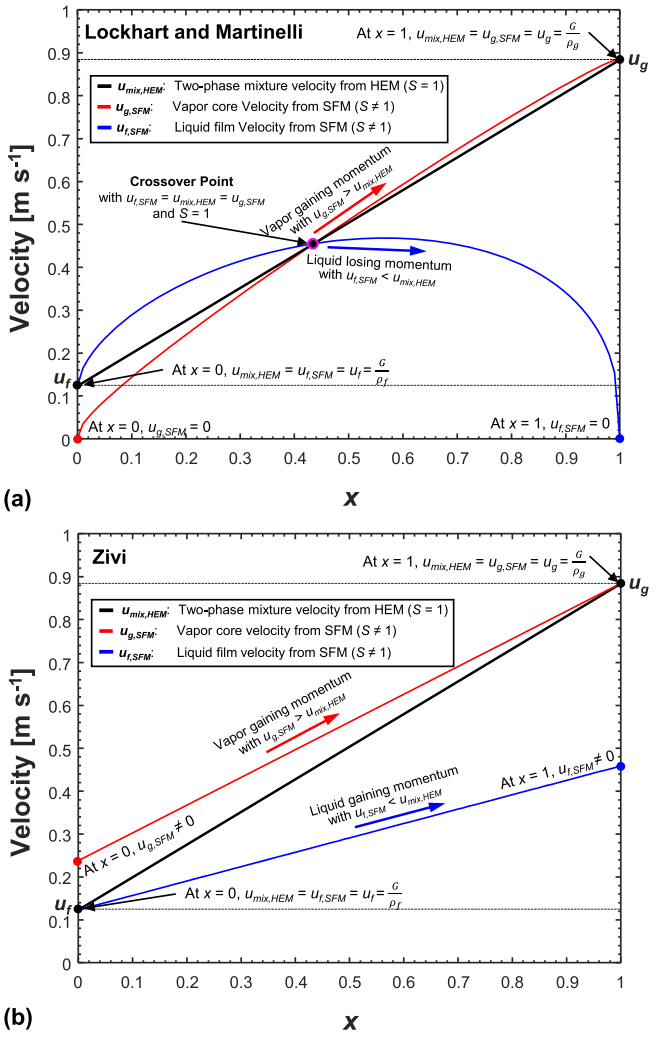

Fig. 6. Assessment of theoretical limits of vapor core and liquid film velocities in separated flow predicted with void fraction relations by (a) Lockhart and Martinelli [45] and (b) Zivi [50] for LH_2 undergoing saturated adiabatic two-phase flow, with $Re_{fo,D} = 5000$, $D = 5$ mm, $P_{R,in} = 0.5$, and flow quality ranging from 0 to 1.

the HEM formulations described in Eqs. (4)–(6) and Table 3.

On the other hand, SFM assumes a finite slip ratio and hence is dependent on semi-empirical relations to estimate the void fraction. Although a detailed review of void fraction models has been performed by Ghajar and Bhagwat [49], this study focuses on the seminal and widely popular void fraction relations by Lockhart and Martinelli [45] and Zivi [50], which are given, respectively,

$$\alpha_{SFM} = \left[1 + \left(\frac{1-x}{x}\right)\left(\frac{\rho_g}{\rho_f}\right)^{2/3}\right]^{-1} \tag{23}$$

and

$$\alpha_{SFM} = \left[1 + 0.28\left(\frac{1-x}{x}\right)^{0.64}\left(\frac{\rho_g}{\rho_f}\right)^{0.36}\left(\frac{\mu_f}{\mu_g}\right)^{0.07}\right]^{-1} \tag{24}$$

The slip ratio, S, corresponding to both these void fraction relations can be found by combining Eqs. (23) and (24) with Eq. (21). The slip ratios according to Lockhart and Martinelli and Zivi's void fraction relations are given, respectively, by Eqs. (25) and (26)

$$S = \frac{u_{g,SFM}}{u_{f,SFM}} = \left(\frac{\rho_g}{\rho_f}\right)^{-1/3} \tag{25}$$

and

$$S = \frac{u_{g,SFM}}{u_{f,SFM}} = 0.28\left(\frac{1-x}{x}\right)^{-0.36}\left(\frac{\rho_g}{\rho_f}\right)^{-0.64}\left(\frac{\mu_f}{\mu_g}\right)^{0.07} \tag{26}$$

With strikingly different functional forms, it is imperative to check which of the two void fraction relations would capture the true fluid physics in a separated flow. Fig. 6 compares theoretical limits for velocities of the vapor core ($u_{g,SFM}$) and liquid film ($u_{f,SFM}$) in separated flow according to the relations by Lockhart and Martinelli and Zivi for LH_2 undergoing saturated adiabatic two-phase flow under idealized operating conditions of $Re_{fo,D} = 5000$, in a 5-mm diameter tube, with an inlet reduced pressure of $P_{R,in} = 0.5$, and with flow quality ranging from 0 to 1. As reference, the two-phase mixture velocity ($u_{mix,HEM}$) based on the HEM model is also shown to check for the limiting conditions of $x = 0$ and 1 (where HEM is valid because of existence of only liquid or only vapor). Derived from mass conservation, also shown in Appendix 1, the analytical expressions for $u_{mix,HEM}$, $u_{f,SFM}$, and $u_{g,SFM}$ are given, respectively, by

$$u_{mix,HEM} = \frac{G}{\rho_{tp}} = G\left(\frac{x}{\rho_g} + \frac{1-x}{\rho_f}\right) \tag{27}$$

$$u_{f,SFM} = \frac{G}{\alpha S \rho_g + (1-\alpha)\rho_f} \tag{28}$$

and

$$u_{g,SFM} = \frac{G}{\alpha \rho_g + \frac{(1-\alpha)}{S}\rho_f} \tag{29}$$

Hence, under the limiting condition of $x = 0$ (saturated liquid), the two-phase mixture velocity converges to saturated single-phase liquid velocity, $u_{mix,HEM} = G/\rho_f = u_f$. Additionally, under the limiting condition of $x = 1$ (saturated vapor), the two-phase mixture velocity converges to saturated single-phase vapor velocity, $u_{mix,HEM} = G/\rho_g = u_g$. Similarly, under the limiting conditions of $\alpha = 0$ at $x = 0$ (flow area occupied by saturated liquid), $u_{f,SFM} = G/\rho_f = u_f$. And under the limiting conditions of $\alpha = 1$ at $x = 1$ (flow area occupied by saturated vapor), $u_{g,SFM} = G/\rho_g = u_g$.

However, for the analytical expressions of phase velocities for separated flows derived in Appendix 1, there are two additional conditions that need to be satisfied under the limiting values of $\alpha = 0$ and $\alpha = 1$. These analytical expressions for the vapor core and liquid film velocities in an idealized annular separated flow are determined by mass conservation and are bounded on the extremities by pure liquid ($\alpha = x = 0$ where $A_f = A$ and $A_g = 0$) and by pure vapor ($\alpha = x = 1$ where $A_f = 0$ and $A_g = A$). When the flow area is completely filled with saturated liquid ($\alpha = 0$ at $x = 0$), in addition to $u_{f,SFM} = G/\rho_f = u_f$, the vapor core velocity should also converge to 0 due to non-existence of an interface, i.e., $u_{g,SFM} = 0$. Similarly, when the flow area is completely filled with saturated vapor ($\alpha = 1$ at $x = 1$), in addition to the condition of $u_{g,SFM} = G/\rho_g = u_g$, the liquid film velocity should also converge to 0, i.e., $u_{f,SFM} = 0$.

It is evident that, while the Lockhart and Martinelli void fraction relation in Fig. 6(a) does satisfy all the aforementioned limiting conditions for phase velocities at both $x = 0$ ($u_{f,SFM} = u_f$ and $u_{g,SFM} = 0$) and $x = 1$ ($u_{f,SFM} = 0$ and $u_{g,SFM} = u_g$), Zivi's relation in Fig. 6(b) only satisfies $u_{f,SFM} = u_f$ at $x = 0$ and $u_{g,SFM} = u_g$ at $x = 1$. Hence, this study adopts Lockhart and Martinelli's void fraction relation, Eq. (24), when calculating the two-phase accelerational and gravitational pressure gradients using the SFM formulations described in Eqs. (7) and (8) and Table 4. Additionally, a very interesting physical inference on the crossover of

Table 5
Data exclusion strategy for single component total pressure drop data for sub-critical saturated cryogenic flow boiling in uniformly heated straight tubes with prescribed inlet conditions.

Reference	Deviation from standard flow configuration[a]	Missing data	Miscellaneous factors	Remarks
(a) Complete Exclusion				
Pope *et al.* [51]		●		Inlet pressure information missing
Jones and Altman [52]	●			Circular test section with a U-bend
Keilin *et al.* [53]		●		Only overall range for mass velocity provided
La Harpe *et al.* [54]	●			Helically coiled tube test section
Jergel and Stevenson [55]	●			Rectangular channel test section with only a small fraction of test section heated
Jergel *et al.* [56]	●			Rectangular channel test section with only a small fraction of test section heated
Steiner and Schlünder [57]		●		Inlet quality information missing
Steiner and Schlünder [58]			●	Repetitive data from Steiner and Schlünder [57]
Deev *et al.* [59]			●	Data points are provided in the form of friction multiplier [c] across the test section
Züst [60]			●	Test section dimensions unclear
Deev *et al.* [61]		●		Inlet quality information missing for certain data points; data points are provided in the form of dimensionless two-phase frictional pressure drop [d] across the test section
Petukhov *et al.* [62]		●	●	Only overall range for mass velocity and inlet quality provided for certain data points; heat flux information missing for certain data points; data points are provided in the form of dimensionless two-phase frictional pressure drop [d] across the test section
Müller *et al.* [63]		●		Inlet quality information missing
Vishnev *et al.* [64]		●		Inlet quality information missing
Mamedov *et al.* [65]			●	Data points are provided in the form of dimensionless two-phase frictional pressure drop [d] across the test section
Gan and Filippov [66]			●	Data points are provided in the form of dimensionless two-phase frictional pressure drop [d] across the test section
Subbotin *et al.* [67]			●	Data points are provided in the form of friction multiplier [c] across the test section
Subbotin *et al.* [68]		●	●	Inlet quality information missing; certain data points provided for decreasing heat flux
Popp and Preclik [69]			●	Repetitive data from Hendricks *et al.* [70]
Huang and Van Sciver [71]			●	Repetitive data from Huang [72]
Filippov [73]		●		Tube diameter information missing
Qi *et al.* [74]		●		Heat flux, inlet quality, and inlet pressure information missing
Rane *et al.* [75]			●	Repetitive data from Vishnev *et al.* [64]
Mustafi [76]	●			Dryout occurred in a helically shaped pre-heater
Deng *et al.* [77]	●			Two-phase flow in heated U-tubes
Dittmar *et al.* [78]	●			Flexible tube test section
Chang *et al.* [79]	●			Flexible tube test section
Chen *et al.* [80]		●		Inlet quality information missing
(b) Partial Exclusion [b]				
Hendricks *et al.* [81]	●			Certain data points provided for supercritical pressures
Mohr and Runge [82]		●		Heat flux and inlet quality information missing for certain data points
Huang [83]			●	Certain data points are provided in the form of friction multiplier [c] or dimensionless two-phase frictional pressure drop [d] across the test section
Van Noord [28]	●		●	Certain data points provided for supercritical pressures; certain data points exhibit negative pressure drop

[a] Standard flow configuration is a uniformly heated straight circular tube with heat applied externally into the single-component fluid.
[b] Select data points were excluded while the remaining have been used in the present study.
[c] To estimate total pressure drop, ΔP_{tp}, from two-phase frictional pressure drop multiplier ($\Delta P_{tp,F}/\Delta P_{sp,fo,F}$), information for single-phase friction factor is required along with the information for void fraction, α, to determine the two-phase accelerational ($\Delta P_{tp,A}$) and two-phase gravitational ($\Delta P_{tp,G}$) pressure drops.
[d] To estimate total pressure drop, ΔP_{tp}, from dimensionless two-phase frictional pressure drop ($\Delta P^{*}_{tp,F} = \frac{\Delta P_{tp,F} - \Delta P_{sp,fo,F}}{\Delta P_{sp,go,F} - \Delta P_{sp,fo,F}}$), information for single-phase friction factor is required along with the information for void fraction, α, to determine the two-phase accelerational ($\Delta P_{tp,A}$) and two-phase gravitational ($\Delta P_{tp,G}$) pressure drops.

vapor core velocity ($u_{g,SFM}$) and liquid film velocity ($u_{f,SFM}$) from SFM with respect to the two-phase mixture velocity ($u_{mix,HEM}$) from HEM is observed in Fig. 6(a). As the flow quality and therefore the void fraction increase, the vapor core gets thicker while the liquid film gets thinner. From mass conservation, the vapor gains momentum along the flow direction as the liquid film loses momentum. Despite the vapor core's momentum gain, it is only beyond the crossover point ($u_{f,SFM} = u_{mix,HEM} = u_{g,SFM}$) that the vapor velocity begins to exceed the two-phase mixture velocity from HEM (i.e., $u_{g,SFM} > u_{mix,HEM}$) and the slip ratio begins to exceed unity (i.e., $u_{g,SFM} > u_{f,SFM}$). Similarly, despite the liquid film's

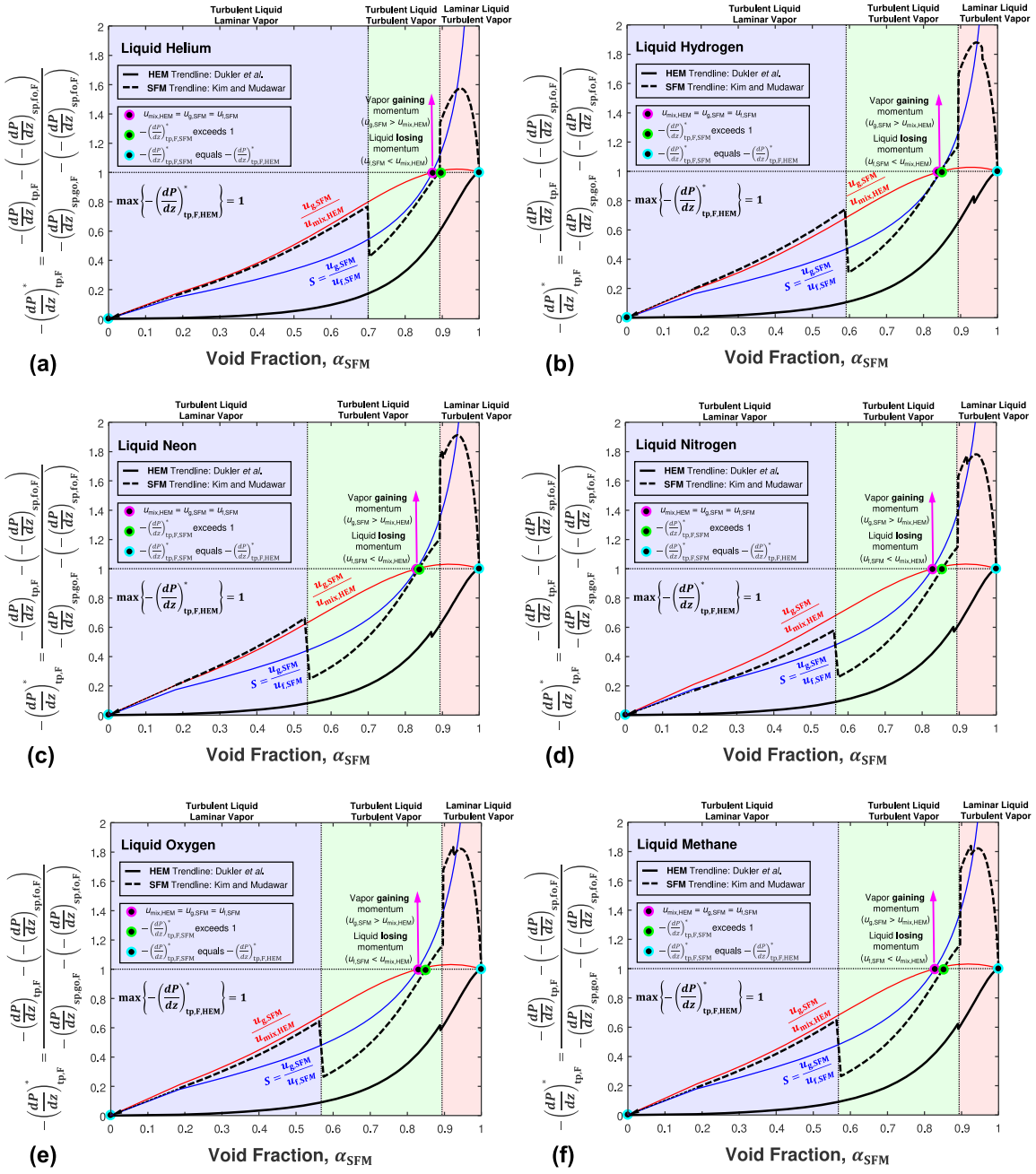

Fig. 7. Variation of dimensionless two-phase frictional pressure gradient with local void fraction for (a) Liquid Helium, (b) Liquid Hydrogen, (c) Liquid Neon, (d) Liquid Nitrogen, (e) Liquid Oxygen, and (f) Liquid Methane for saturated adiabatic two-phase flow with $Re_{fo,D} = 5000$, $D = 5$ mm, and $P_{R,in} = 0.5$, using both HEM with relation by Dukler *et al.* [42] and SFM with semi-empirical formulation by Kim and Mudawar [37].

momentum loss, it is only beyond the crossover point that the liquid film velocity drops below the two-phase mixture velocity from HEM (i.e., $u_{f,SFM} < u_{mix,HEM}$) and the slip ratio exceeds unity (i.e., $u_{g,SFM} > u_{f,SFM}$). Overall, both these trends beyond the crossover point strongly allude to separated flow physics encountered at void fractions high enough to create significant momentum in the thick vapor core and a slip ratio greater than unity. The significance of the crossover point in demarcating dispersed flow dominant cryogenic data from separated flow dominant data will be explained in a later section.

3. Compilation of PU-BTPFL Cryogenic Pressure Drop Database

As indicated earlier, the present study involves exhaustive mining of total pressure drop data for saturated two-phase flow of cryogens from all literature sources available to the present authors. This included (i) major cryogen journals (e.g., Cryogenics (Elsevier), Advances in Cryogenic Engineering (Springer), (ii) major cryogen conferences (e.g., International Cryogenic Engineering Conference), (iii) NASA and NIST technical reports, and (iv) other sporadic publications, reports, and theses from across the globe.

Total pressure drop data are extracted only from references with clearly prescribed inlet conditions, i.e., $\Delta P_T = f(q, P_{in}, x_{e,in}, G, D, L_H)$. For the two-phase flow data, in order to ensure that the experimental two-phase frictional pressure drop is accurately evaluated using Eq. (20), experimental data reported in the form of either two-phase frictional pressure drop multiplier ($\Delta P_{tp,F}/\Delta P_{sp,fo,F}$) or dimensionless two-phase frictional pressure drop $\left(\frac{\Delta P_{tp,F} - \Delta P_{sp,fo,F}}{\Delta P_{sp,go,F} - \Delta P_{sp,fo,F}}\right)$ are not included in the

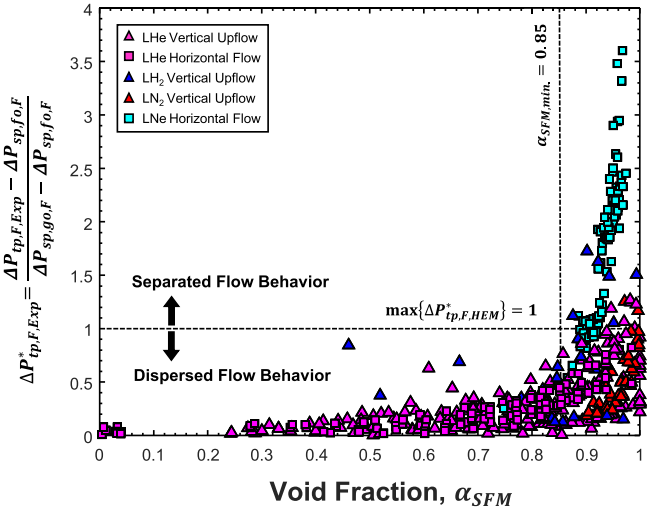

Fig. 8. Application of proposed demarcation of dispersed flow dominant from separated flow dominant data against both saturated adiabatic liquid-vapor flow data and saturated flow boiling data using the dimensionless two-phase frictional pressure drop in the present PU-BTPFL Cryogenic Pressure Drop Database.

database, due to missing information for single-phase friction factor.

Four kinds of total pressure drop data are extracted: (i) total pressure drop across a *heated* tube undergoing *single-phase flow* satisfying one of two criteria, $x_{e,in} < 0$ with $x_{e,out} < 0$ for pure subcooled liquid single-phase flow, and $x_{e,in} > 1$ with $x_{e,out} > 1$ for pure superheated vapor single-phase flow, (ii) total pressure drop across an *unheated* tube undergoing *single-phase flow* satisfying one of two criteria, $x_{e,in} = x_{e,out} = 0$ for pure saturated liquid single-phase flow, and $x_{e,in} = x_{e,out} = 1$ for pure saturated vapor single-phase flow, (iii) total pressure drop across an *unheated* tube undergoing saturated *adiabatic liquid-vapor two-phase flow* satisfying the criteria $0 \leq x_{e,in} = x_{e,out} \leq 1$, and (iv) total pressure drop across a *heated* tube undergoing *saturated flow boiling* satisfying both the limiting criteria for saturated region of $x_{e,in} < 1$ (*upper limit*) and $x_{e,out} > 0$ (*lower limit*). Since both dispersed and separated flow features can be observed even in post-CHF regions, both dispersed/mist flow post-Dryout type CHF and inverted annular flow post-DNB type CHF, saturated boiling data incurring CHF within the saturated boiling region are also included in the database. The single-phase flow data are used exclusively to validate the single-phase frictional pressure gradient relations, Eqs. (14) and (15a-c), while the saturated two-phase flow data are used to develop a new correlation method for cryogenic two-phase frictional pressure gradient.

The data mining effort is complicated by difficulty acquiring certain references because of such factors as (a) lack of availability from international interlibrary services, (b) reluctance of a few investigators to share their own data, and (c) lack of English translated versions of foreign literature with data. Avoidance of duplicate data is a thorough and time-consuming effort, necessitated by the fact that many published works lack clear indication of sources for the data presented. Overall, the possibility of data duplication in the total pressure drop database is prevented by careful point-by-point inspection of the acquired data.

After completing the initial data mining effort and making certain of absence of duplicate data, efforts shifted to excluding data that do not strictly conform to the following uniformity requirements:

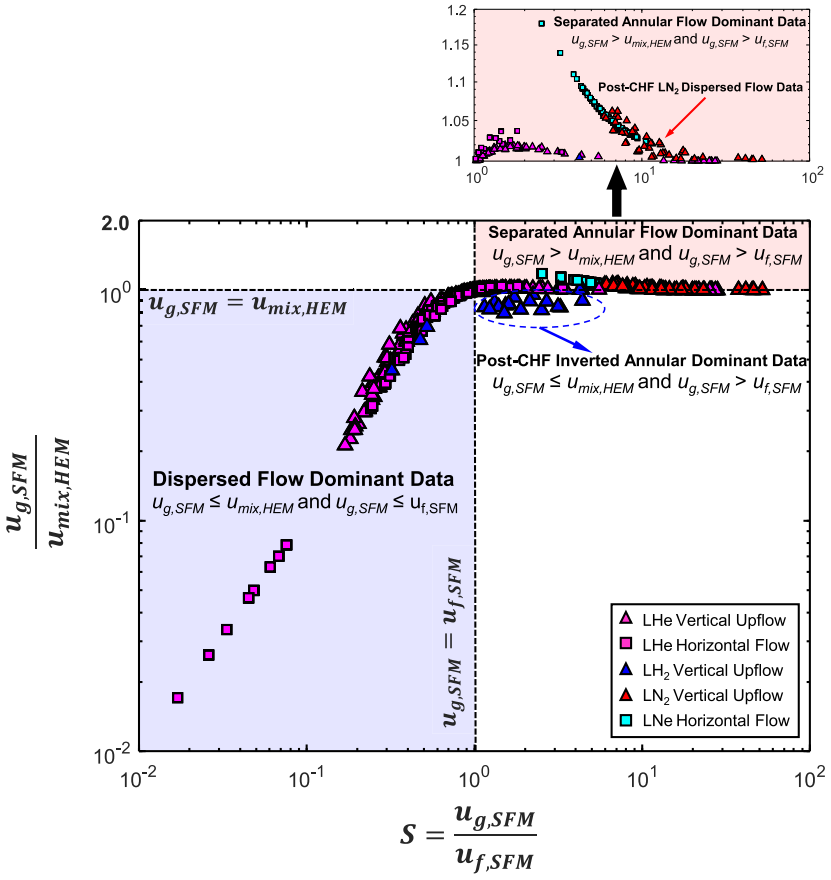

Fig. 9. Application of proposed demarcation of dispersed flow dominant from separated flow dominant data against both saturated adiabatic liquid-vapor flow data and saturated flow boiling data using relevant velocity ratios in the present PU-BTPFL Cryogenic Pressure Drop Database.

Table 6
Summary of physics-based classifiers to demarcate dispersed flow dominant region from separated flow dominant region for acceptable data in the PU-BTPFL Cryogenic Pressure Drop (ΔP_T) Database.

Reference	Acceptable ΔP_T data points	Reduced Pressure P_R	Void Fraction α_{out} [a]	Liquid Reynolds Number $Re_{f,D,out}$ x 10^{-3}	Vapor Reynolds Number $Re_{g,D,out}$ x 10^{-3}	Proposed Classifiers Evaluated at the Outlet: $\Delta P^*_{tp,F,Exp}$ [b]	$\frac{\Delta z_{sat,tot.}}{L_H}$ [c]	$\frac{u_{g,SFM}}{u_{f,SFM}}$ [d]	$\frac{u_{g,SFM}}{u_{mix,HEM}}$ [e]	Remarks
Saturated Adiabatic Two-Phase Flow										
Liquid Helium										
Khalil [84]	96	0.47 0.91	0.27 0.99	1.1 143.2	2.5 296.4	0.04 1.27	- [c] - [c]	0.19 5.52	0.25 1.02	Brass tube Orientation [f]: **VU** State [g]: adiabatic two-phase Flow [h]: **vt, tt**
Huang [83]	110	0.29 0.53	0.004 0.98	2.3 102.7	0 214	0.01 0.82	- [c] - [c]	0.02 3.34	0.02 1.04	Brass tube Orientation [f]: **H** State [g]: adiabatic two-phase Flow [h]: **tv, tt**
Liquid Neon										
Mohr & Runge [82]	2	0.06 0.06	0.75 0.87	3 3.9	8.8 26.5	0.25 0.66	- [c] - [c]	2.53 4.1	1.10 1.18	SF-Copper tube Orientation [f]: **H** State [g]: adiabatic two-phase Flow [h]: **tt**
Saturated Flow Boiling										
Liquid Helium										
Khalil [84]	117	0.49 0.89	0.24 0.99	0 137	1.5 334	0.004 1.006	0.144 1.125	0.169 28.08	0.21 1.02	Brass tube Orientation [f]: **VU** State [g]: Pre-CHF saturated boiling Flow [h]: **vt, tt, tv**
Liquid Hydrogen										
Hendricks *et al.* [70]	17	0.14 0.38	0.76 0.97	137 1068	1066.5 3712	0.126 1.49	0.692 1.198	1.147 4.405	0.795 0.956	Inconel tube Orientation [f]: **VU** State [g]: Post-CHF inverted annular film boiling Flow [h]: **tt**
Hendricks *et al.* [81]	8	0.43 0.86	0.46 0.99	13.4 1795	288.8 6322.2	0.375 1.725	0.119 0.886	0.32 4.25	0.45 1.011	Inconel, Inconel X, SS304 tubes Orientation [f]: **VU** State [g]: Post-CHF inverted annular film boiling Flow [h]: **tt**
Liquid Neon										
Mohr & Runge [82]	79	0.056 0.056	0.82 0.97	0.5 3.6	16.5 85.7	0.312 3.602	1.291 > 1000	3.267 10.55	1.024 1.139	SF-Copper tube Orientation [f]: **H** State [g]: Pre-CHF saturated soiling Flow [h]: **vt, tt**
Liquid Nitrogen										
Laverty & Rohsenow [85]	41	0.034 0.042	0.90 0.99	0 11.5	52.5 370.2	0.185 1.253	1.001 1.009	5.97 52.06	1.002 1.062	SS304 tube Orientation [f]: **VU** State [g]: Post-CHF dispersed flow film boiling Flow [h]: **vt, tt**
Forslund & Rohsenow [86]	4	0.05 0.051	0.95 0.99	0 4.7	139.1 257.2	0.237 0.847	0.947 0.974	7.624 46.103	1.002 1.035	SS304 tube Orientation [f]: **VU** State [g]: Post-CHF dispersed flow film boiling Flow [h]: **vt, tt**

[a] Void fraction at the outlet evaluated using the relation by Lockhart and Martinelli [45].

[b] The dimensionless two-phase frictional pressure drop is defined as $\Delta P^*_{tp,F,Exp} = \frac{\Delta P_{tp,F,Exp} - \Delta P_{sp,fo,F}}{\Delta P_{sp,go,F} - \Delta P_{sp,fo,F}}$, where the two-phase frictional pressure drop ($\Delta P_{tp,F,Exp}$) is evaluated using Eq. (20). The void fraction defined in Eq. (22) is used to predict the gravitational and accelerational (only for boiling data) pressure drop components for HEM formulation.

[c] The total saturation length ratio for saturated flow boiling is defined as $\frac{\Delta z_{sat,tot.}}{L_H} = \frac{\min\{x_{e,out}, 1\}}{4Bo}\left(\frac{L_H}{D}\right)^{-1}$. For adiabatic liquid-vapor two-phase flows with two-phase mixture inlet, total saturation length ratio is defined as $\frac{\Delta z_{sat,tot.}}{L_{PH}} = \frac{\min\{x_{e,out,PH}, 1\}}{4Bo_{PH}}\left(\frac{L_{PH}}{D}\right)^{-1}$. Due to no pre-heater information, this value is undetermined for adiabatic two-phase flow data in this study.

[d] The saturated vapor core velocity at the outlet of the tube in an idealized separated flow ($u_{g,SFM}$) as defined in Eq. (29). The saturated liquid film velocity at the outlet of the tube in an idealized separated flow ($u_{f,SFM}$) as defined in Eq. (28).

[e] The two-phase mixture velocity at the outlet of the tube in an idealized homogeneous flow ($u_{mix,HEM}$) as defined in Eq. (27).

[f] **VU**: vertical upflow; **H**: horizontal flow.

[g] State of the fluid in the saturated two-phase flow section of the tube.
[h] **vt**: laminar liquid ($Re_f < 2000$) – turbulent vapor ($Re_g \geq 2000$); **tv**: turbulent liquid ($Re_f \geq 2000$) – laminar vapor ($Re_g < 2000$); **tt**: turbulent liquid ($Re_f \geq 2000$) – turbulent vapor ($Re_g \geq 2000$).

Table 7
Summary of saturated boiling data points excluded from the PU-BTPFL Cryogenic Two-Phase Pressure Drop Database.

Reference	Total ΔP_T data points	Limiting Conditions for $\Delta P^*_{tp,F,exp}$ [a]		Non-Equilibrium Condition $x_{e,out} > 1$ but $x_{out} < 1$	Acceptable ΔP_T data points
		$\Delta P^*_{tp,F,exp} < 0$	$\Delta P^*_{tp,F,exp} > 2$		
Liquid Helium					
Khalil [84]	122	5			117
Liquid Hydrogen					
Hendricks *et al.* [70]	20	2	1		17
Hendricks *et al.* [81]	26		17	1 [b]	8
Liquid Neon					
Mohr and Runge [82]	82		0 [c]	3 [d]	79
Liquid Nitrogen					
Laverty and Rohsenow [85]	60		6	13 [e]	41
Forslund and Rohsenow [86]	39	12	13	10 [e]	4
Liquid Methane					
Van Noord [28]	4	1	3		0
Total	**353**	**20**	**40**	**27**	**266**

[a] Limiting conditions for the dimensionless two-phase frictional pressure drop, $\min\{\Delta P^*_{tp,F}\} = 0$ and $\max\{\Delta P^*_{tp,F}\} = 2$, where $\Delta P^*_{tp,F} = \frac{\Delta P_{tp,F} - \Delta P_{sp,fo,F}}{\Delta P_{sp,go,F} - \Delta P_{sp,fo,F}}$. These inferences are made from Figs. 7(a)–(f).
[b] Applicable to post-CHF data by Hendricks et al. [81] for inverted annular film boiling with strong non-equilibrium ($x \neq x_e$).
[c] 32 data points by Mohr and Runge [82] with $\Delta P^*_{tp,F} > 2$ are nevertheless included in the database because of the possibility to attain this condition due to high-quality two-phase mixture inlet conditions with total saturation length ratio, $\Delta z_{sat,tot.}/L_H > 1.3$ even for pre-CHF data, where $\frac{\Delta z_{sat,tot.}}{L_H} = \frac{\min\{x_{e,out},1\}}{4Bo}\left(\frac{L_H}{D}\right)^{-1}$.
[d] Applicable to pre-CHF data by Mohr and Runge [82] for two-phase mixture inlet conditions and saturated flow boiling with possible non-equilibrium ($x \neq x_e$) leading to $x_{out} > 1$ for pre-CHF data.
[e] Applicable to post-CHF data by Laverty and Rohsenow [85] and Forslund and Rohsenow [86] for dispersed flow film boiling with strong non-equilibrium ($x \neq x_e$).

(1) Only single-component cryogens; data for binary or higher order mixtures are excluded.
(2) Only forced convection driven flow in tubes; data for boiling in capillary tubes, thermosyphons, and natural circulation systems are excluded.
(3) Flow in only straight circular tubes; data for non-circular test sections (e.g., rectangular, square, annular, rod, bundle), helical tubes or U-bends are excluded.
(4) Flow in only stationary tubes; data for rotating tubes are excluded.
(5) Flow not involving use of a swirl flow promotor (e.g., twisted tape, wire coil inserts) within the tube or upstream of the tube's inlet.
(6) Flow not involving use of abnormal test section inlet or outlet (e.g., orifice plate, inlet expansion, outlet expansion).
(7) Only data for vertical upflow, vertical downflow, and horizontal flow; data for inclines tubes are excluded.
(8) Only uniformly heated circular tubes; data for axially or circumferentially nonuniform wall heat flux are excluded.
(9) Only steady state data; transient boiling data are excluded.
(10) Only fully wetted tube data; horizontal flow boiling in stratified and stratified-wavy flow regimes are rejected.
(11) Only pressure drop data presented by original authors with documented values for every parameter necessary for correlating the data (e.g., heat flux, operating pressure, mass velocity, inlet quality, tube geometry, *etc.*) are considered.

This exclusion strategy, details of which are summarized in Table 5, resulted in an initial database suitable for developing correlations (also future models) for the saturated flow boiling frictional pressure gradient specific to cryogens. However, it is important to note that the above do not constitute a complete list for data exclusions, as other considerations, achieved through further assessment of the amassed data as discussed in the next section, preclude inclusion of certain additional datapoints. These additional exclusions are used in pursuit of the final PU-BTPFL Cryogenic Pressure Drop Database.

4. Assessment of PU-BTPFL Cryogenic Pressure Drop Database

Pursuant to application of the exclusion criteria discussed in the previous section, further assessment of cryogenic total pressure drop data is broadly classified into two categories based on implementation of (i) demarcation criteria for dispersed from separated flow and (ii) physics-based data exclusion criteria.

4.1. Demarcation Criteria for Dispersed from Separated Flow

The two-phase frictional gradient within the saturated length or two-phase length, L_{tp}, can be normalized by representing it as dimensionless two-phase frictional pressure gradient, $-(dP/dz)^*_{tp,F}$, which is defined as

$$-\left(\frac{dP}{dz}\right)^*_{tp,F} = \frac{-\left(\frac{dP}{dz}\right)_{tp,F} - \left(-\left(\frac{dP}{dz}\right)_{sp,fo,F}\right)}{-\left(\frac{dP}{dz}\right)_{sp,go,F} - \left(-\left(\frac{dP}{dz}\right)_{sp,fo,F}\right)} \tag{30}$$

where $-(dP/dz)_{sp,fo,F}$ represents the hypothetical single-phase liquid frictional pressure gradient over the same two-phase length assuming only saturated liquid flow over L_{tp}. Similarly, $-(dP/dz)_{sp,go,F}$ represents the hypothetical single-phase vapor frictional pressure gradient over the same two-phase length assuming only saturated vapor flow over L_{tp}.

This hypothesis is a consequence of the HEM based formulation for determining the two-phase frictional pressure gradient, as described in Eqs. (4)-(5a-c). At the limit of $x = 0$ (saturated liquid), Eq. (4) simplifies to its *minimum* value corresponding to saturated liquid single-phase frictional pressure gradient.

$$-\left(\frac{dP}{dz}\right)_{tp,F}\Bigg|_{x=0} = \frac{2f_{sp,fo}G^2}{\rho_f D} = -\left(\frac{dP}{dz}\right)_{sp,fo,F} \tag{31}$$

Similarly, at the limit of $x = 1$ (saturated vapor), Eq. (4) simplifies to

Table 8
Pure single-phase liquid and single-phase vapor total pressure drop (ΔP_{sp}) data for cryogens.

Reference	Acceptable ΔP_T data points	Tube dimensions		Inlet and Operating Conditions				ΔP_{sp} Measurements		Remarks
		D x 10^3 [m]	L_H/D [a]	P_{in} x 10^{-6} [N m^{-2}]	G [kg m^{-2} s^{-1}]	q x 10^{-3} [W m^{-2}]	$x_{e,in}$	ΔP_{sp} x 10^{-3} [N m^{-2}]	$\frac{\Delta P_{sp}}{P_{in}} \times 100$ [%]	
Adiabatic Pure Single-Phase Data										
Liquid Helium										
Khalil [84]	18	2.13	366.3	0.107	41	0	0	1.26	0.63	Brass tube
		2.73	469.5	0.207	165.58	0	0	2.28	1.96	Orientation [b]: **VU**
										State [c]: pure saturated liquid single-phase
Khalil [84]	15	2.13	366.3	0.107	41	0	1	0.58	0.47	Brass tube
		2.73	469.5	0.207	165.58	0	1	6.34	5.67	Orientation [b]: **VU**
										State [c]: pure saturated vapor single-phase
Liquid Nitrogen										
Forslund & Rohsenow [86]	6	8.2	148.6	0.17	56.8	0	2.05	1.88	1.1	SS304 Tube
		8.2	148.6	0.172	162.1	0	2.18	14.5	8.5	Orientation [b]: **VU**
										State [c]: pure superheated vapor single-phase
	39									
Diabatic Pure Single-Phase Data										
Liquid Helium										
Khalil [84]	12	2.13	366.3	0.119	41	0.026	−0.54	1.27	0.69	Brass tube
		2.73	469.5	0.204	168.1	0.397	−0.016	2.19	1.62	Orientation [b]: **VU**
										State [c]: pure subcooled liquid single-phase
	12									
Total	**51**									

[a] For adiabatic single-phase flows, the heated length (L_H) is the same as the length of the tube across which the pressure drop is measured.
[b] **VU**: vertical upflow.
[c] State of the fluid throughout the tube from inlet to outlet.

its *maximum* value corresponding to saturated vapor single-phase frictional pressure gradient.

$$-\left(\frac{dP}{dz}\right)_{tp,F}\Bigg|_{x=1} = \frac{2f_{sp,go}G^2}{\rho_g D} = -\left(\frac{dP}{dz}\right)_{sp,go,F} \tag{32}$$

Thus, as the flow quality, x, increases from 0 to 1, the dimensionless two-phase frictional pressure gradient, $-(dP/dz)^*_{tp,F}$, is normalized between 0 and 1 when using HEM. Mathematically, at $x = 0$, $-(dP/dz)^*_{tp,F} = 0$, and at $x = 1$, $-(dP/dz)^*_{tp,F} = 1$.

With respect to SFM formulation, although the limiting conditions at $x = 0$ and $x = 1$, given by Eq. (31) and Eq. (32), respectively, hold true, as the flow quality increases from 0 to 1, the dimensionless two-phase frictional pressure gradient can exhibit values greater than 1 at intermediate flow qualities due to the presence of a separated flow whose physics are best captured by the semi-empirical SFM formulations described in Table 4. A physical argument for this behavior of $-(dP/dz)^*_{tp,F} > 1$ when using SFM is the presence of a vapor core thick enough to gain momentum where the two-phase frictional pressure gradient caused by this high vapor core velocity now starts to exceed the hypothetical single-phase vapor frictional gradient at the same flow quality, i.e., $-(dP/dz)_{tp,F} > -(dP/dz)_{sp,go,F}$. A similar physical argument was observed in Fig. 6(a) and discussed in Section 2.4. For phase velocities predicted using the slip ratio relation by Lockhart and Martinelli [45], it is only beyond the crossover point ($u_{f,SFM} = u_{mix,HEM} = u_{g,SFM}$) that the vapor core velocity would exceed the two-phase mixture velocity from HEM ($u_{g,SFM} > u_{mix,HEM}$) and the slip ratio would exceed unity ($u_{g,SFM} > u_{f,SFM}$), all of which strongly suggest separated flow dominant features.

This hypothesis is put to test in Fig. 7 where the dimensionless two-phase frictional pressure gradients from both the HEM formulation by Dukler *et al.* [42] and the SFM formulation by Kim and Mudawar [37] are plotted against void fraction spanning 0 to 1. This analysis is performed for all commonly used cryogens undergoing saturated adiabatic two-phase flow at $Re_{fo,D} = 5000$ in a 5-mm diameter tube with inlet reduced pressure, $P_{R,in} = 0.5$. On the same plots, both $u_{g,SFM}/u_{mix,HEM}$ and slip ratio, $S = u_{g,SFM}/u_{f,SFM}$, are also plotted following Eqs. (27)–(29). Since this study adopts Lockhart and Martinelli's [45] void fraction relation, all the SFM terms including phase velocities and void fraction are also based on Lockhart and Martinelli. It can be seen that both HEM and SFM satisfy Eq. (32) at the limiting condition of $\alpha = 1$. At the limiting condition of $\alpha = 0$, HEM satisfies Eq. (31) while SFM asymptotically converges to Eq. (31). It can also be seen that HEM follows the normalized trend of dimensionless two-phase frictional pressure gradient having values between 0 and 1 for both flow quality and void fraction ranging from 0 to 1. However, for SFM, although the dimensionless two-phase frictional pressure gradient does lie between 0 and 1, there comes a point usually in the turbulent-liquid turbulent-vapor region (*tt*) or in the laminar-liquid turbulent-vapor region (*vt*), where it exceeds unity before eventually converging to unity at $\alpha = 1$. This transition of $-(dP/dz)_{tp,F,SFM}$ beyond unity is also closely captured by the slip ratio which also exceeds unity; this is where the vapor core gains enough momentum to exceed the two-phase mixture velocity from HEM, i.e., $u_{g,SFM} > u_{mix,HEM}$. These trends are consistent irrespective of cryogen but specific to the conditions used in Fig. 7, i.e., $Re_{fo,D} = 5000$, $D = 5$ mm, and $P_{R,in} = 0.5$. Hence, from the presented trends it is reasonable to infer that where the dimensionless two-phase frictional pressure gradient exceeds unity, the flow is most certainly separated. On the other hand, where the dimensionless two-phase frictional pressure gradient is less that unity, the flow is most likely dispersed. Similarly, from the same trends it is also reasonable to infer that, where slip ratio exceeds unity and $u_{g,SFM} > u_{mix,HEM}$, the flow is more likely separated.

These criteria for demarcating dispersed flow dominant data from

Table 9
Parameter ranges of acceptable total pressure drop (ΔP_T) data in the PU-BTPFL Cryogenic Pressure Drop Database.

Reference	Acceptable ΔP_T data points	Tube dimensions		Inlet and Operating Conditions				ΔP_T Measurements		Remarks
		D x 10^3 [m]	L_H/D [a]	P_{in} x 10^{-6} [N m^{-2}]	G [kg m^{-2} s^{-1}]	q x 10^{-3} [W m^{-2}]	$x_{e,in}$	ΔP_T x 10^{-3} [N m^{-2}]	$\frac{\Delta P_T}{P_{in}} \times 100$ [%]	
Saturated Adiabatic Liquid-Vapor Flow										
Liquid Helium										
Khalil [84]	96	2.13 2.73	366.3 469.5	0.107 0.207	41 165.58	0 0	0.011 0.99	0.55 6.32	0.46 5.66	Brass tube Orientation [b]: **VU** State [c]: adiabatic two-phase Flow [d]: **vt, tt**
Huang [83]	110	4.57 5.33	126.4 211.9	0.066 0.122	31.96 73.53	0 0	0 0.97	0.02 0.21	0.02 0.26	Brass tube Orientation [b]: **H** State [c]: adiabatic two-phase Flow [d]: **tv, tt**
Liquid Neon										
Mohr & Runge [82]	2	4 4	22 22	0.15 0.15	116 120	0 0	0.08 0.25	0.057 0.13	0.04 0.09	SF-Copper tube Orientation [b]: **H** State [c]: adiabatic two-phase Flow [d]: **tt**
Saturated Flow Boiling										
Liquid Helium										
Khalil [84]	117	2.13 2.73	366.3 469.5	0.112 0.204	41 168.1	0.016 2.41	−0.574 0.001	0.80 3.91	0.66 3.5	Brass tube Orientation [b]: **VU** State [c]: Pre-CHF saturated boiling Flow [d]: **vt, tt, tv**
Liquid Hydrogen										
Hendricks *et al.* [70]	17	7.95 7.95	38.2 38.2	0.188 0.498	575.65 1626.44	374.24 1650.59	−0.12 0.026	38.61 179.26	20.5 44.1	Inconel tube Orientation [b]: **VU** State [c]: Post-CHF inverted annular film boiling Flow [d]: **tt**
Hendricks *et al.* [81]	8	4.77 12.88	37.5 101.1	0.562 1.113	531.94 2735.4	294.16 1732.3	−0.378 −0.09	19.99 159.96	2.38 19.51	Inconel, Inconel X, SS304 tubes Orientation [b]: **VU** State [c]: Post-CHF inverted annular film boiling Flow [d]: **tt**
Liquid Neon										
Mohr & Runge [82]	79	4 4	22 75	0.15 0.15	75.2 140	0.001 47.62	0.08 0.71	0.074 1.966	0.05 1.31	SF-Copper tube Orientation [b]: **H** State [c]: Pre-CHF saturated boiling Flow [d]: **vt, tt**
Liquid Nitrogen										
Laverty & Rohsenow [85]	41	8.10 8.10	149.8 149.8	0.115 0.143	94.53 299.73	11.8 82.97	0 0	2.55 19.72	2.17 13.79	SS304 Tube Orientation [b]: **VU** State [c]: Post-CHF dispersed flow film boiling Flow [d]: **vt, tt**
Forslund & Rohsenow [86]	4	5.79 11.73	207.8 421	0.17 0.174	95.33 259.98	16.65 30.32	−0.053 −0.025	4.25 15.7	2.5 9.14	SS304 Tube Orientation [b]: **VU** State [c]: Post-CHF dispersed flow film boiling Flow [d]: **vt, tt**

[a] For adiabatic liquid-vapor flows, the heated length (L_H) is the same as the length of the tube across which the pressure drop is measured.
[b] **VU**: vertical upflow; **H**: horizontal flow.
[c] State of the fluid in the saturated two-phase flow section of the tube.
[d] **vt**: laminar liquid ($Re_f < 2000$) – turbulent vapor ($Re_g \geq 2000$); **tv**: turbulent liquid ($Re_f \geq 2000$) – laminar vapor ($Re_g < 2000$); **tt**: turbulent liquid ($Re_f \geq 2000$) – turbulent vapor ($Re_g \geq 2000$).

separated flow dominant data are put to test in Figs. 8 and 9. In Fig. 8, the dimensionless two-phase frictional pressure drop, $\Delta P^*_{tp,F}$, defined as

$$\Delta P^*_{tp,F} = \frac{\Delta P_{tp,F} - \Delta P_{sp,fo,F}}{\Delta P_{sp,go,F} - \Delta P_{sp,fo,F}} \tag{33}$$

is plotted against exit void fraction to identify separated flow dominant data in the PU-BTPFL Cryogenic Pressure Drop Database. It can be seen that for $\alpha_{SFM} > 0.85$ the LNe data by Mohr and Runge [82] and LH_2 data by Hendricks *et al.* [70,81] show $\Delta P^*_{tp,F} > 1$, thereby alluding to separated flow dominant features. These inferences are also confirmed in Fig. 9. Although this criterion ($\Delta P^*_{tp,F} > 1$) is useful in demarcating dispersed flow dominant data at *low* exit void fractions and separated flow dominant data at *high* exit void fractions, it is not sufficient to demarcate flow regimes for high exit void fraction data with $\Delta P^*_{tp,F} < 1$ which could be associated with either post-CHF dispersed/mist flow regimes or pre-CHF intermittent flow regimes. In Fig. 9, where $u_{g,SFM}/u_{mix,HEM}$ is plotted against the slip ratio, $S = u_{g,SFM}/u_{f,SFM}$, both evaluated at the exit, the demarcation is more evident for dispersed flow dominant data as having $u_{g,SFM}/u_{mix,HEM} \leq 1$ and $S \leq 1$. Whereas for separated flow dominant data, the converse is true with $u_{g,SFM}/u_{mix,HEM} > 1$ and $S > 1$. Consistent with the inference from Fig. 8, both the LNe and LH_2 data show separated flow physics with $S > 1$. However, the LH_2

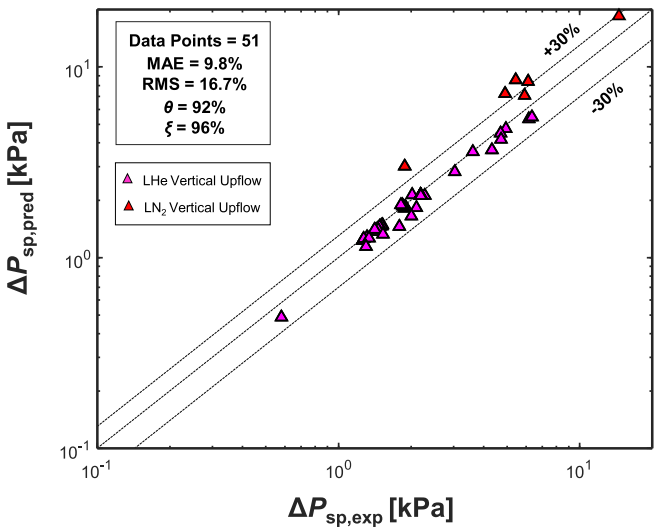

Fig. 10. Predicted versus measured single-phase total pressure drop for cryogenic data in the PU-BTPFL Cryogenic Pressure Drop Database, with subcooled liquid, saturated liquid, saturated vapor,and superheated vapor inlet conditions.

data by Hendricks *et al.* [70,81] show that $u_{g,SFM}/u_{mix,HEM} \leq 1$. This is because they are associated with post-CHF inverted annular flow regime where the vapor film is not thick enough and the liquid core is not thin enough to allow the vapor velocity to gain enough momentum to exceed that of the two-phase HEM mixture. Additionally, it is seen that LN_2 data by Laverty and Rohsenow [85] and Forslund and Rohsenow [86], both associated with post-CHF dispersed/mist flow regimes, show $S > 1$ and $u_{g,SFM}/u_{mix,HEM} > 1$. This is true because of high vapor momentum associated with dispersed/mist flow post-Dryout type CHF for Laverty and Rohsenow [85] and because of inverted annular flow regime prevailing post-DNB (Departure from Nucleate Boiling) type CHF for Forslund and Rohsenow [86] before transitioning to dispersed/mist flow.

Finally, a very unique experimental feature exists for the LNe data by Mohr and Runge [82]. With use of pre-heaters and throttle valve upstream of their test section, their data have been shown by Ganesan *et al.* [34] as having an exorbitantly high total saturation length ratio, which is defined as

$$\frac{\Delta z_{\text{sat,tot.}}}{L_{\text{H}}} = \frac{z_{x_e=\min\{x_{\text{e,out}},1\}} - z_{x_e=0}}{L_H} = \frac{\min\{x_{\text{e,out}},1\}}{4Bo}\left(\frac{L_{\text{H}}}{D}\right)^{-1} \tag{34}$$

where, $z_{x_e=0}$ corresponds to the location from inlet where local x_e becomes zero, and L_H is the heated length of the tube. It has been hypothesized by Ganesan *et al.* [34] that $\Delta z_{sat,tot}/L_H \leq 1.1$ for nominal inlet conditions. However, the LNe data show values consistently greater than 1.3 with some even exceeding 1000. This behavior is unique to the manner in which the experiments were conducted by Mohr and Runge [82] that enabled attaining high flow quality separated flows as indicated in Figs. 8 and 9. Table 6 shows a summary of the physics-based classifiers developed in this study to demarcate dispersed flow dominant data from separated flow dominant data and applied to the final PU-BTPFL Cryogenic Pressure Drop Database.

4.2. Physics-Based Data Exclusion Criteria

The limiting conditions for the dimensionless two-phase frictional pressure drop, $\Delta P^*_{tp,F}$, are estimated from the limiting conditions for the dimensionless two-phase frictional pressure gradient, $-(dP/dz)^*_{tp,F}$. From Fig. 7, it is evident that the lower limit of $-(dP/dz)^*_{tp,F}$ is 0 whereas the upper limit does exceed 1 for separated flows. However, on plotting the dimensionless two-phase frictional pressure gradient for all the SFM

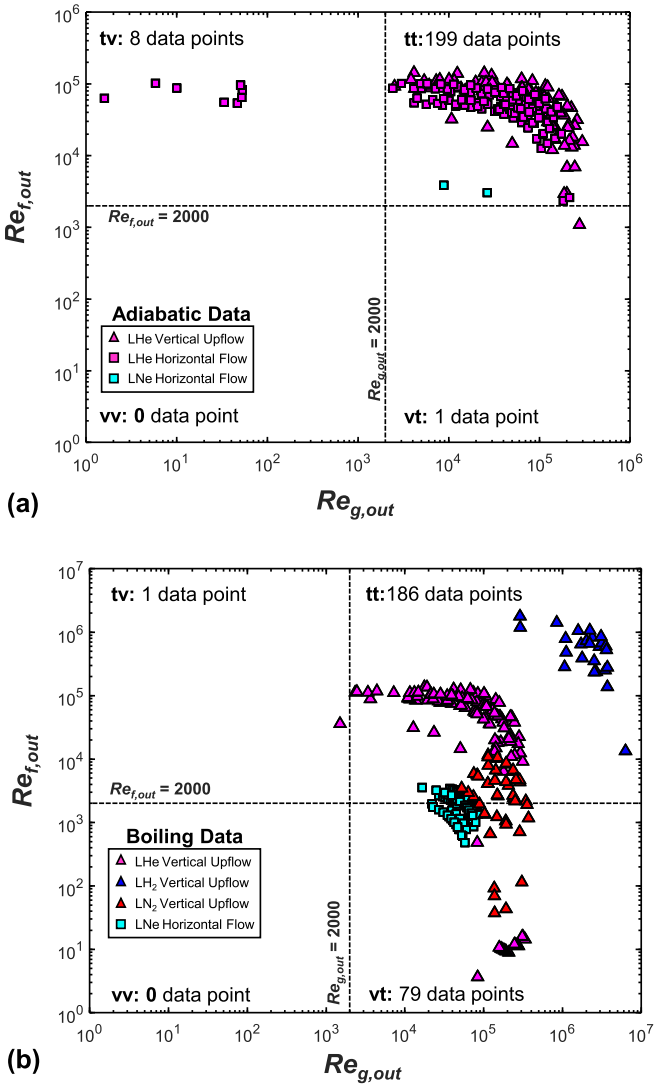

Fig. 11. Laminar/turbulent flow distribution map of consolidated (a) saturated adiabatic liquid-vapor two-phase flow data and (b) saturated flow boiling data from the PU-BTPFL Cryogenic Pressure Drop Database based on superficial liquid and vapor Reynolds number at the outlet.

based semi-empirical formulations tabulated in Table 4, it is observed that the maximum value of $-(dP/dz)^*_{tp,F}$ never exceeds 2 for SFM correlations by Kim and Mudawar [37], Friedel [46] and Müller-Steinhagen and Heck [47]. Although the value of $-(dP/dz)^*_{tp,F}$ for SFM correlation by Lockhart and Martinelli [45] does exceed 2 at higher reduced pressures, a conservative upper limit condition for $-(dP/dz)^*_{tp,F}$ and thus $\Delta P^*_{tp,F}$ is set to 2. Mathematically, the limiting conditions for the dimensionless two-phase frictional pressure drop proposed in this study are: $\min\{\Delta P^*_{tp,F}\} = 0$ and $\max\{\Delta P^*_{tp,F}\} = 2$, where $\Delta P^*_{tp,F}$ is defined in Eq. (33). Table 7 provides details of data points that were excluded for violating these limits.

In the current study, the region of non-equilibrium before the saturated boiling length, $z_{x_e=0} - z_{x=0}$, is merged with the single-phase liquid region. Similarly, the region of non-equilibrium after the saturated boiling length, $z_{x=1} - z_{x_e=1}$, is merged with the single-phase vapor region. Hence, any data having strong non-equilibrium ($x \neq x_e$) are excluded from the database. Table 7 provides details of data points that were excluded for exhibiting non-equilibrium condition at the outlet of the heated tube where the thermodynamic equilibrium quality exceeded unity ($x_{e,out} > 1$), but the flow was reported to be two-phase throughout

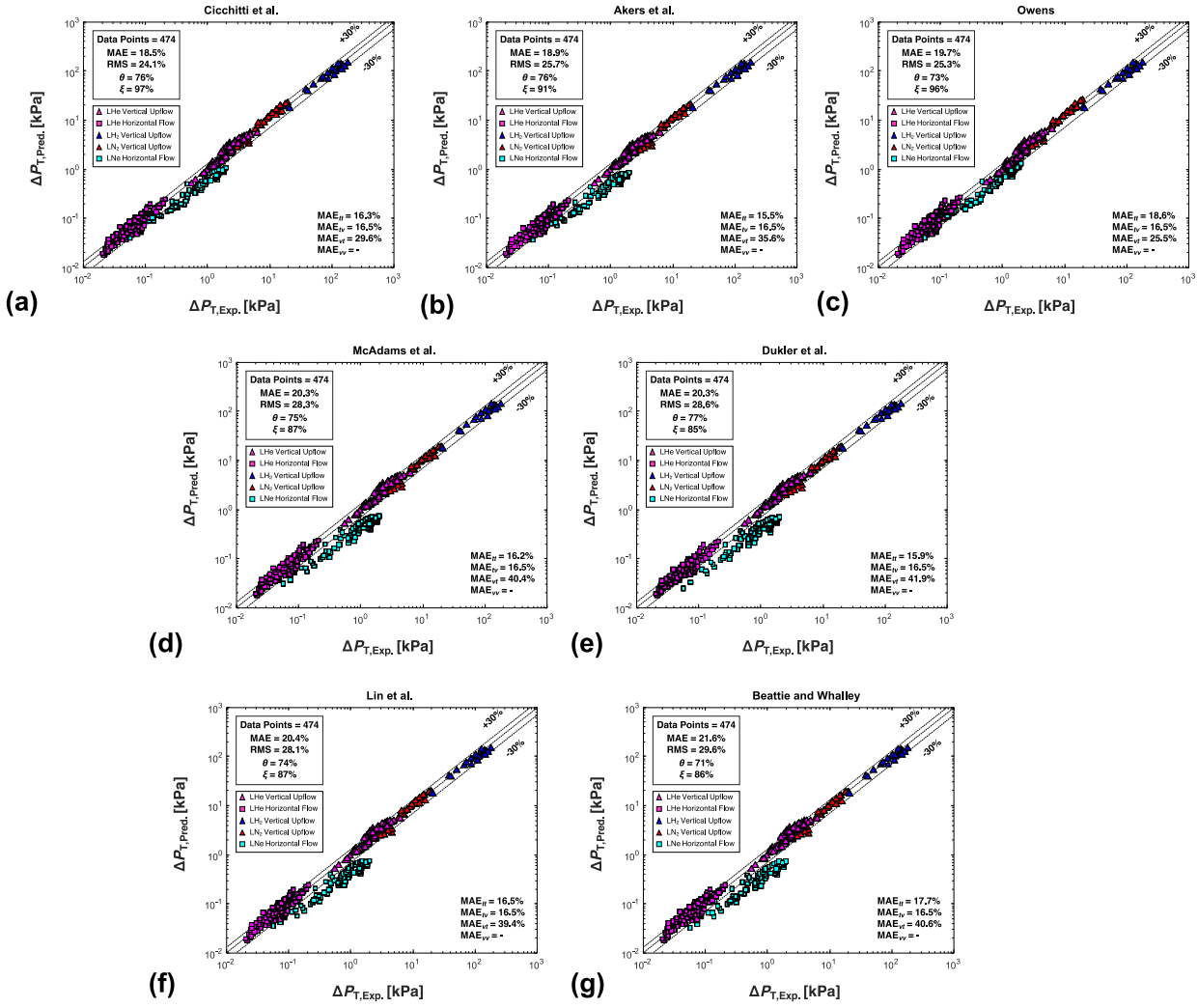

Fig. 12. Comparison of 474 experimental ΔP_T datapoints, including both saturated adiabatic liquid-vaporflow and saturated flow boiling, with HEM predictions wherein the frictional pressure drop component is calculated using two-phase mixture viscosity models by (a) Cicchitti *et al.* [40], (b) Akers *et al.* [39], (c) Owens [41], (d) McAdams *et al.* [38], (e)Dukler *et al.* [42], (f) Lin *et al.* [43], and (g) Beattie and Whalley [44]. The void fraction defined in Eq. (22) is used to predict the gravitational and accelerational components of pressure drop; the latter being zero for adiabatic flow.

the tube ($0 < x_{out} < 1$).

4.3. PU-BTPFL Cryogenic Pressure Drop Database

The final PU-BTPFL Cryogenic Pressure Drop Database, which includes all data deemed acceptable for development of saturated two-phase pressure gradient correlations, is arrived at after applying all the exclusion criteria outlined in the Sections 4.1 and 4.2. A relatively limited total pressure drop database for tubes with pure single-phase liquid and single-phase vapor flows (pure single-phase subcooled liquid, saturated liquid, saturated vapor, superheated vapor) along the entire tube are tabulated in Table 8. It comprises 51 useable single-phase total pressure drop data points. Complete details of the two-phase total pressure drop database are provided in Table 9 (208 total pressure drop data for saturated adiabatic liquid-vapor two-phase flow and 266 total pressure drop data for saturated flow boiling). Overall, it is comprised of 474 useable ΔP_T data points conforming to both the Homogeneous Equilibrium Model formulation as described in Eqs. (4) and (5a) to (5c) and the Separated Flow Model formulation as described in Table 4, and therefore acceptable for correlation development.

Overall, the database encompasses four different fluids: liquid helium, LHe, liquid hydrogen, LH_2, liquid neon, LNe, and liquid nitrogen, LN_2. In Table 9, upper and lower numbers for each parameter represent minimum and maximum values, respectively, for acceptable ΔP_T data corresponding to a particular reference. With a total of 474 data points, it is the largest database ever consolidated from the literature for cryogens containing both adiabatic liquid-vapor and saturated boiling (pre-CHF and post-CHF) two-phase flow pressure drop data.

5. Development of Universal Two-Phase Pressure Gradient Correlations

Before developing the two-phase frictional pressure gradient correlations, it is imperative to test the accuracy of the single-phase friction factor, f_{sp}, for accurate estimation of $\Delta P_{tp,F,exp}$. Fig. 10 shows the total pressure drop for pure single-phase flow data listed in Table 8 with $\Delta P_T = \Delta P_{sp}$. The single-phase total pressure drop is predicted using Eq. (13) with a Mean Absolute Error (MAE) of 9.8 % and a Root Mean Squared (RMS) error of 16.7 %. The MAE and RMS are defined, respectively, as

$$MAE = \frac{1}{N}\sum \frac{\left|\Delta P_{T,pred} - \Delta P_{T,exp}\right|}{\Delta P_{T,exp}} \times 100\% \tag{35}$$

and

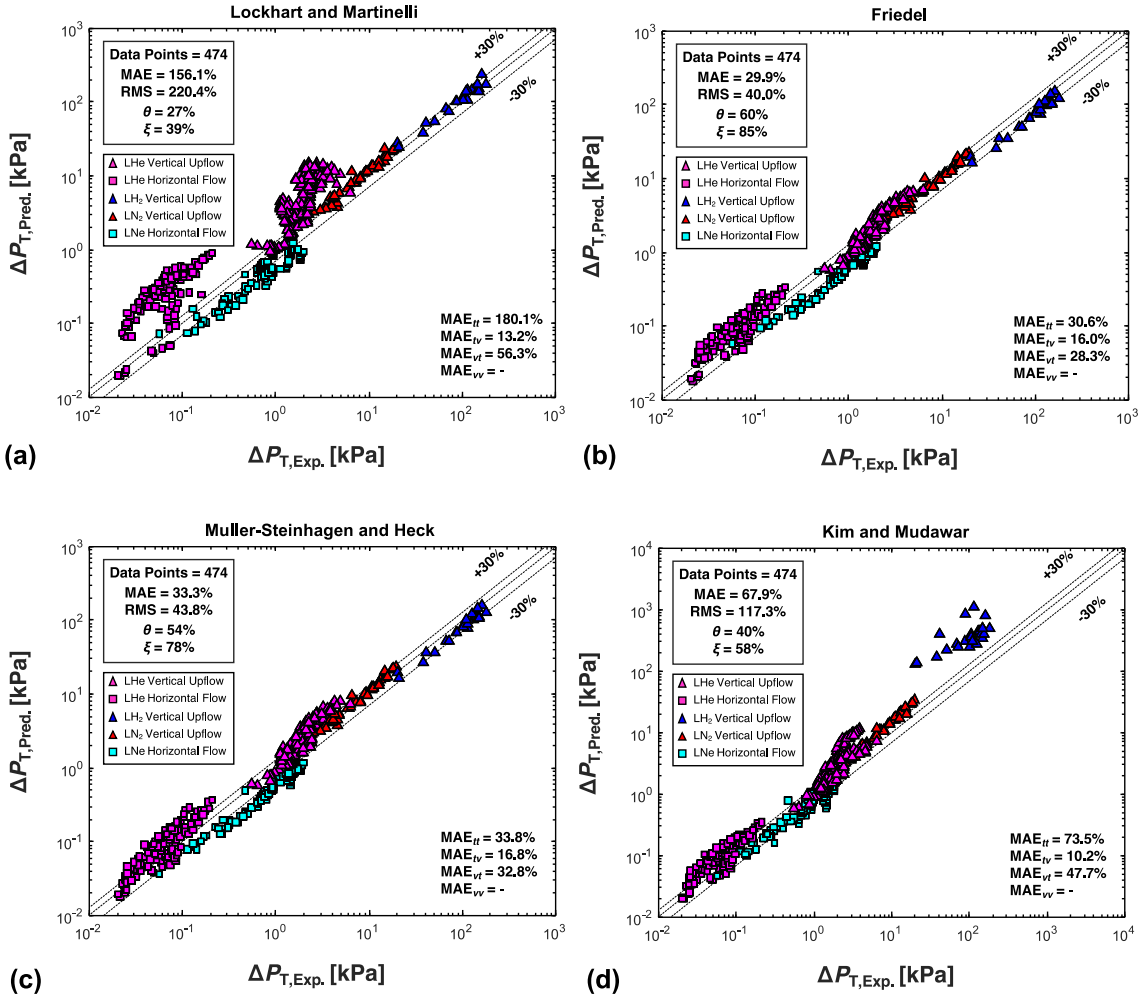

Fig. 13. Comparison of 474 experimental ΔP_T datapoints, including both saturated adiabatic liquid-vapor flow and saturated flow boiling, with SEM predictions based on semi-empirical formulations of (a) Lockhart and Martinelli [45], (b) Friedel [46], and (c) Muller-Steinhagen and Heck [47] and (d) Kim and Mudawar [37]. The void fraction defined in Eq. (24) is used to predict the gravitational and accelerational components of pressure drop; the latter being zero for adiabatic flow.

$$RMS = \sqrt{\frac{1}{N}\sum\left(\frac{\Delta P_{T,pred} - \Delta P_{T,exp}}{\Delta P_{T,exp}}\right)^2} \times 100\% \tag{36}$$

Fig. 11 shows the flow distributions corresponding to two-phase data in the PU-BTPFL Cryogenic Pressure Drop Database which are tested against seminal HEM and SFM formulations.

Fig. 12 shows how HEM formulations provide good predictions for all cryogens except LNe, for the entire PU-BTPFL Cryogenic Pressure Drop Database consisting of 474 datapoints. This is because the LNe data from Mohr and Runge [82], by virtue of having high saturation length ratio, also exhibits strong separated flow features as shown earlier in Figs. 8 and 9. Hence, the most important classifier that separates LNe data from the rest is the total saturation length ratio, and HEM is applicable only for $\Delta z_{sat,tot}/L_H < 1.2$. It is important to note that, while Cicchitti *et al.* [40] shows the lowest MAE of all HEM two-phase viscosity models, excluding the LNe data, best accuracy is achieved with the viscosity model of Dukler *et al.* [42]. Additionally, the hypothesis made in Section 1.2 on the unique behavior of LHe obeying the Homogenous Equilibrium Model even for separated flow dominant data is proven right from Figs. 9 and 12.

Fig. 13 shows a comparizon with predictions from semi-empirical SFM formulations, for the entire PU-BTPFL Cryogenic Pressure Drop Database. While this figure, might point to the Friedel's correlation [46], by virtue of its lowest MAE of 29.9 %, as providing best overall accuracy among SFM correlations, it masks the influence of the most significant classifier that separates LNe data from the rest, namely total saturation length ratio, with SFM applicable only for $\Delta z_{sat,tot}/L_H \geq 1.2$. With focus on the LNe data alone, the SFM correlation method by Kim and Mudawar [37] provides the most accurate predictions among the SFM formulations. Here as well, the hypothesis made in Section 1.2 on the unique behavior of LNe obeying the Separated Flow Model owing to a stable separated, annular flow regime is proven right from Figs. 9 and 13.

Hence, using only the total saturation length ratio, $\Delta z_{sat,tot}/L_H$, as demarcator, a hybrid HEM-SFM method is proposed wherein HEM correlation method is used in conjunction with the two-phase mixture viscosity relation by Dukler *et al.* [42] for $\Delta z_{sat,tot}/L_H < 1.2$ (393 data points), shown separately in Fig. 14(a), while the SFM correlation method by Kim and Mudawar [37] is used for $\Delta z_{sat}/L_H \geq 1.2$ (81 data points), shown separately in Fig. 14(b). The reason for using only the total saturation length ratio as demarcator is the excellent performance of HEM correlations for $\Delta z_{sat,tot}/L_H < 1.2$. Also, the reason to choosing Kim and Mudawar's SFM correlation [37] is its excellent predictive capability for $\Delta z_{sat,tot}/L_H \geq 1.2$, which encompasses only LNe data. As shown in Fig. 14(c), with an MAE of 14.7 % irrespective of cryogenic fluid or flow orientation, the hybrid HEM-SFM method provides very good agreement with the data.

The use of the total saturation length ratio, $\Delta z_{sat,tot}/L_H$, to demarcate dispersed flow dominant data from separated flow dominant data for

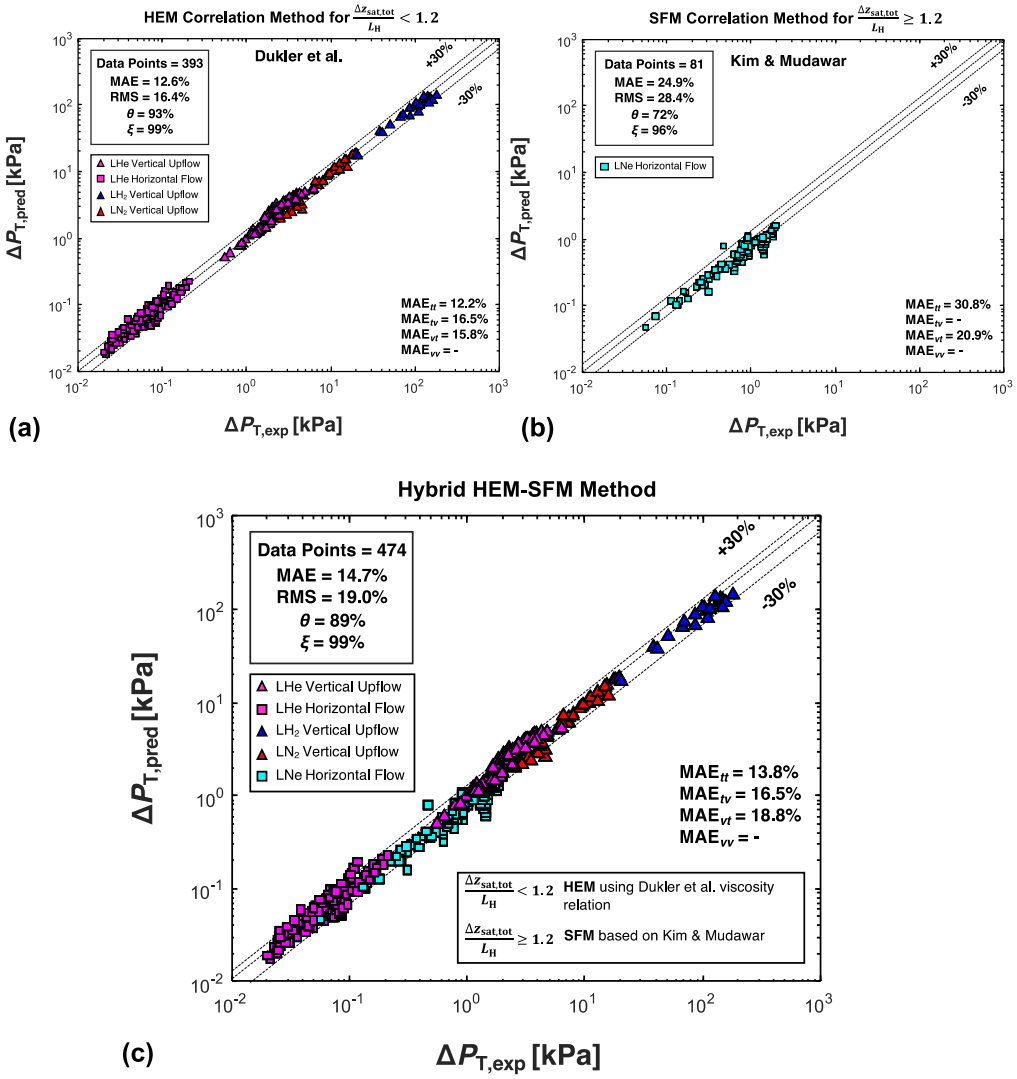

Fig. 14. Comparison of predictions of total pressure drop using (a) HEM correlation method for $\frac{\Delta z_{sat,tot}}{L_H} < 1.2$, (b) SFM correlation method for $\frac{\Delta z_{sat,tot}}{L_H} \geq 1.2$, and (c) hybrid HEM-SFM method against both adiabatic liquid-vapor flow and saturated flow boiling data from the PU-BTPFL Cryogenic Pressure Drop Database.

saturated flow boiling pressure drop prediction is further justified by the heat transfer coefficient trends observed by Ganesan *et al.* [34] for saturated flow boiling. It was observed that under nominal inlet conditions with saturation length ratio ≤ 1.1, the heat transfer mechanism within the saturated boiling region was nucleate boiling dominant. However, for high quality two-phase mixture inlet conditions with saturation length ratio > 1.1, evidence of strong convective boiling heat transfer mechanism was observed. Since the flow regime within a heated tube is strongly interlinked with the heat transfer mechanism, the resulting inference of observing *dispersed flow dominant* flow regime during *nucleate boiling dominant* heat transfer for lower saturation length ratio and *separated flow dominant* flow regime during *convective boiling dominant* heat transfer is consistent with the coupled thermo-fluidic boiling physics.

As indicated earlier, two additional goals of this study are to (i) identify *gaps* in the available data which warrant further experimental investigation, and (ii) recommend a methodology for acquiring future ΔP_T data in a manner that is conducive to refining two-phase frictional pressure gradient correlations and/or mechanistic models. Fig. 11 points to major gaps in the laminar-liquid and laminar-vapor flow ranges (*vv*), with cryogenic data essentially absent from it. Also, despite having an abundance of LHe data, there is significant dearth of total pressure drop data for other cryogens. It is also recommended that for fluids such as LOX and LCH_4, there needs to be proper tests conducted to get total pressure drop data. Future work can also benefit from better understanding of pressure drop in the non-equilibrium region upstream of location of $z_{x_e=0}$, which has been shown to depart from single-phase pressure drop calculations in a study involving HFE 7100 [87].

It is also important to note that the work described in this study concerns adiabatic flow and flow boiling of cryogens in mostly macro-tubes important to space applications. From a fundamental standpoint regarding other applications of cryogens, future work is recommended to address pressure drop in capillary flows (e.g., [88]), micro-channel flows (e.g., [87,89]), and more complex two-phase flows (e.g., [90]), as well as effects of instabilities on pressure drop in flow boiling (e.g., [91]).

6. Conclusions and Recommendations

The present study is motivated by the absence of a reliable, error-free saturated flow boiling pressure drop database for developing and validating two-phase frictional pressure gradient correlations as well as future analytic and computational models. An exhaustive literature search identified 474 useful saturated two-phase total pressure drop

data points for four different fluids, viz., LHe, LH_2, LNe, and LN_2, and acceptable data were consolidated into a single PU-BTPFL Cryogenic Pressure Drop Database. An exhaustive parametric study of the database was performed to gain insight into the fluid physics unique to cryogens, and to aid future investigators into important operating conditions where there is a dearth of data. Finally, using the database, frictional pressure gradient correlations were constructed for two distinct inlet conditions of nominal inlet conditions and high-quality inlet conditions based on the total saturation length ratio, which required careful physics-based demarcation of the data. A new hybrid HEM-SFM correlation method for predicting frictional pressure gradient is recommended, which shows good agreement with the data in terms of both predictive accuracy and trend.

Author Declaration

We wish to confirm that there are no known conflicts of interest associated with this publication and there has been no significant financial support for this work that could have influenced its outcome.

We confirm that the manuscript has been read and approved by all named authors and that there are no other persons who satisfied the criteria for authorship but are not listed. We further confirm that the order of authors listed in the manuscript has been approved by all of us.

We confirm that we have given due consideration to the protection of intellectual property associated with this work and that there are no impediments to publication, including the timing of publication, with respect to intellectual property. In so doing we confirm that we have followed the regulations of our institutions concerning intellectual property.

We understand that the Corresponding Author is the sole contact for the Editorial process (including Editorial Manager and direct communications with the office). He/she is responsible for communicating with the other authors about progress, submissions of revisions and final approval of proofs. We confirm that we have provided a current, correct email address which is accessible by the Corresponding Author and which has been configured to accept email from mudawar@ecn.purdue.edu

Declaration of Competing Interest

The authors declare the following financial interests/personal relationships which may be considered as potential competing interests: Issam Mudawar reports financial support was provided by NASA. Jason Hartwig reports a relationship with NASA that includes: employment.

Data availability

All data already provided in manuscript.

Acknowledgements

The authors are grateful for financial support provided by the National Aeronautics and Space Administration (NASA) under grant no. 80GRC018C0055. The authors would also like to acknowledge the services provided by Purdue Libraries, especially its Interlibrary Loan (ILL) service, for helping acquire literature from across the world.

Appendix 1

For saturated flow inside a tube with a mass velocity of G through a flow area of A, mass conservation gives,

$$\rho u A = GA = \text{const.} \tag{A1.1}$$

Under HEM assumptions, Eq. (A1.1) is simplified to Eq. (A1.2) leading to the definition of two-phase mixture velocity, $u_{mix,HEM}$, in Eq. (A1.3).

$$\rho_{tp} u_{mix,HEM} = G \tag{A1.2}$$

$$u_{mix,HEM} = \frac{G}{\rho_{tp}} = \frac{G}{\alpha_{HEM}\rho_g + (1-\alpha_{HEM})\rho_f} = G\left(\frac{x}{\rho_g} + \frac{1-x}{\rho_f}\right) \tag{A1.3}$$

Under SFM assumptions, where the liquid and vapor flow through their respective flow areas of A_f and A_g with phase velocities of $u_{f,SFM}$ and $u_{g,SFM}$ respectively, Eq. (A1.1) is simplified to Eq. (A1.4).

$$\rho_g u_{g,SFM} A_g + \rho_f u_{f,SFM} A_f = GA \tag{A1.4}$$

Applying the definition of void fraction, α, based on flow areas, $\alpha = A_g/A$ and using the relation $A_g + A_f = A$, Eq. (A1.4) simplifies to Eq. (A1.5) for a separated flow.

$$\rho_g u_{g,SFM}\alpha + \rho_f u_{f,SFM}(1-\alpha) = G \tag{A1.5}$$

Finally, introducing the slip ratio, $S = u_{g,SFM}/u_{f,SFM}$, Eq. (A1.5) is simplified to Eq. (A1.6) leading to the definition of vapor-phase velocity, $u_{g,SFM}$, in Eq. (A1.7) within the respective vapor flow area, A_g, of a separated flow.

$$\rho_g u_{g,SFM}\alpha + \rho_f \frac{u_{g,SFM}}{S}(1-\alpha) = G \tag{A1.6}$$

$$u_{g,SFM} = \frac{G}{\alpha\rho_g + \frac{(1-\alpha)}{S}\rho_f} \tag{A1.7}$$

Similarly, Eq. (A1.5) is simplified to Eq. (A1.8) leading to the definition of liquid-phase velocity, $u_{f,SFM}$, in Eq. (A1.9) within the respective liquid flow area, A_f, of a separated flow.

$$\rho_g S u_{f,SFM}\alpha + \rho_f u_{f,SFM}(1-\alpha) = G \tag{A1.8}$$

$$u_{f,SFM} = \frac{G}{\alpha S \rho_g + (1-\alpha)\rho_f} \tag{A1.9}$$

References

[1] G. Hildebrandt, Heat transfer to boiling helium-I under forced flow in a vertical tube, in: Proceedings of the 4th International Cryogenic Engineering Conference, 1972, pp. 295–300.
[2] P.J. Giarratano, R.C. Hess, M.C. Jones, Forced convection heat transfer to subcritical helium I, Nat. Bureau Stand. Rep. (1973), 73-322.
[3] H. Ogata, S. Sato, Critical heat flux for two-phase flow of helium I, Cryogenics 13 (1973) 610–611 (Guildf).
[4] H. Ogata, S. Sato, Forced convection heat transfer to boiling helium in a tube, Cryogenics 14 (1974) 375–380 (Guildf).
[5] B.S. Petukhov, V.M. Zhukov, V.M. Shieldcret, Investigation of heat transfer and hydrodynamics in the helium two-phase flow in a vertical channel. Advanced Course in Heat Exchangers: Theory and Practice, ICHMT Symposium, 1981, pp. 251–262.
[6] V.P. Beliakov, V.A. Shaposhnikov, S.P. Gorbatchev, I.I. Michailov, E.D. Mikitenko, Studies on nucleate boiling crisis of helium-I in channels of superconducting magnet systems, IEEE Trans. Magnet. 15 (1979) 40–45.
[7] V.I. Romanov, A.L. Sevryugin, Yu.M. Pavlov, V.I. Antipov, Investigating burnouts with helium boiling in a channel, Teploenergetika 28 (1981) 620–622.
[8] V.V. Arkhipov, S.V. Kvasnyuk, V.I. Deev, V.K. Andreev, An experimental investigation and method of calculation of critical heat loads when boiling helium in tubes, Teploenergetika 26 (1979) 27–29.
[9] V.I. Deev, V.I. Petrovichev, A.I. Pridantsev, Yu.V. Gordeev, V.V. Arkhipov, V. V. Parygin, Hydraulic resistance and burnout with helium boiling in tubes, Teploenergetika 26 (1979) 45–47.
[10] V.I. Subbotin, V.I. Deev, V.V. Arkhipov, Critical heat flux in flow boiling of helium, Int. Heat Transfer Conf. (1982) 357–361. Digital Library.
[11] V.I. Subbotin, V.I. Deev, A.I. Pridantsev, V.K. Andreev, V.V. Arkhipov, V. N. Novikov, A.N. Savin, V.V. Solodovnikov, Heat transfer and hydrodynamics in cooling channels of superconducting devices, Cryogenics 25 (1985) 261–265 (Guildf).
[12] B.S. Petukhov, V.M. Zhukov, S.B. Anisimov, Cryogenic liquids forced boiling heat transfer in a rotating channel, Cryogenics 26 (1986) 226–233 (Guildf).
[13] T.C. Core, J.F. Harkee, B. Misra, K. Sato, Heat-transfer studies, aerojet-general corporation technical document TID/SNA-164, 1959.
[14] C.C. Wright, H.H. Walters, Single Tube Heat Transfer Tests—Gaseous and Liquid Hydrogen, Wright Air Development Center, 1959. Technical Report 59-423.
[15] J.P. Lewis, J.H. Goodykoontz, J.F. Kline, Boiling heat transfer to liquid hydrogen and nitrogen in forced flow, NASA Tech. 1314 (1962). Note D.
[16] Y. Shirai, H. Tatsumoto, M. Shiotsu, K. Hata, H. Kobayashi, Y. Naruo, Y. Inatani, DNB heat flux on inner side of a vertical pipe in forced flow of liquid hydrogen and liquid nitrogen, Cryogenics 92 (2018) 105–117 (Guildf).
[17] H. Tatsumoto, Y. Shirai, M. Shiotsu, K. Hata, H. Kobayashi, Y. Naruo, Y. Inatani, T. Kato, K. Kinoshita, Forced convection heat transfer of subcooled liquid hydrogen in a small tube, in: Proceedings of the 23rd Engineering Conference and International Cryogenic Materials Conference, 2010, pp. 491–496.
[18] Y. Shirai, H. Tatsumoto, K. Hata, M. Shiotsu, H. Kobayashi, Y. Naruo, Y. Inatani, Preliminary study on heat transfer characteristics of liquid hydrogen for coolant of HTC superconductors, In AIP Conf. Proc. 1218 (2010) 337–339.
[19] H. Tatsumoto, Y. Shirai, M. Shiotsu, K. Hata, H. Kobayashi, Y. Naruo, Y. Inatani, T. Kato, M. Futakawa, K. Kinoshita, Development of a thermal-hydraulics experimental system for high Tc superconductors cooled by liquid hydrogen, J. Phys. Conf. Ser. 234 (2010), 032056.
[20] Y. Shirai, H. Tatsumoto, M. Shiotsu, K. Hata, H. Kobayashi, Y. Naruo, Y. Inatani, K. Kinoshita, Forced flow boiling heat transfer of liquid hydrogen for superconductor cooling, Cryogenics 51 (2011) 295–299 (Guildf).
[21] Y. Shirai, M. Shiotsu, H. Kobayashi, T. Takegami, H. Tatsumoto, K. Hata, H. Kobayashi, Y. Naruo, Y. Inatani, K. Kinoshita, DNB heat flux in forced flow of subcooled liquid hydrogen under pressures, In AIP Conf. Proc. 1434 (2012) 1067–1074.
[22] H. Tatsumoto, Y. Shirai, M. Shiotsu, K. Hata, Y. Naruo, H. Kobayashi, Y. Inatani, K. Kinoshita, Forced convection heat transfer of liquid hydrogen through a 200-mm long heated tube, Phys Proc. 36 (2012) 1360–1365.
[23] H. Tatsumoto, Y. Shirai, M. Shiotsu, K. Hata, Y. Naruo, H. Kobayasi, Y. Inatani, Forced convection heat transfer of saturated liquid hydrogen in vertically-mounted heated pipes, In AIP Conf. Proc 1573 (2014) 44–51.
[24] T. Matsumoto, Y. Shirai, M. Shiotsu, K. Fujita, Y. Iwami, Y. Naruo, H. Kobayashi, S. Nonaka, Y. Inatani, Film boiling heat transfer properties of liquid hydrogen flowing inside of heated pipe, In IOP Conf. Ser. Mater. Sci. Eng. 502 (2019), 012090.
[25] H. Tatsumoto, Y. Shirai, M. Shiotsu, K. Hata, Y. Naruo, H. Kobayashi, Y. Inatani, K. Kinoshita, Forced convection heat transfer of subcooled liquid hydrogen in horizontal tubes, In AIP Conf. Proc 1434 (2012) 747–754.
[26] H. Tatsumoto, Y. Shirai, K. Hata, T. Kato, M. Futakawa, M. Shiotsu, Forced convection heat transfer of subcooled liquid nitrogen in a vertical tube, In J. Phys. Conf. Series 234 (2010), 032057.
[27] H. Tatsumoto, Y. Shirai, K. Hata, T. Kato, M. Shiotsu, Forced convection heat transfer of subcooled liquid nitrogen in horizontal tube, In AIP Conf. Proc 985 (2008) 665–672.
[28] J. Van Noord, A heat transfer investigation of liquid and two-phase methane, NASA Tech. Memo. (2010), 2010-216918.
[29] A. Trejo, M.J. Galvan, A.G. Trujillo, A.R. Choudhuri, Experimental investigation of liquid methane convection and boiling in rocket engine cooling channels, in: Proceedings of the In 50th AIAA/ASME/SAE/ASEE Joint Propulsion Conference, 2014, pp. 4007–4022.
[30] A. Trejo, C. Garcia, A. Choudhuri, Experimental investigation of transient forced convection of liquid methane in a channel at high heat flux conditions, Exp. Heat Transf. 29 (2016) 97–112.
[31] A. Trejo, A. Trujillo, M. Galvan, A. Choudhuri, J.C. Melcher, J.J. Bruggemann, Experimental investigation of methane convection and boiling in rocket engine cooling channels, J. Thermophys. Heat Transf. 30 (2016) 937–945.
[32] E.W. Lemmon, I.H. Bell, M.L. Huber, M.O. McLinden, NIST Standard Reference Database 23: Reference fluid Thermodynamic and Transport properties-REFPROP, Version 10.0, Standard Reference Data Program, NIST, Gaithersburg, 2018.
[33] V. Ganesan, R. Patel, J. Hartwig, I. Mudawar, Universal critical heat flux (CHF) correlations for cryogenic flow boiling in uniformly heated tubes, Int. J. Heat Mass Transfer 166 (2021), 120678.
[34] V. Ganesan, R. Patel, J. Hartwig, I. Mudawar, Review of databases and correlations for saturated flow boiling heat transfer coefficient for cryogens in uniformly heated tubes, and development of new consolidated database and universal correlations, Int. J. Heat Mass Transfer 179 (2021), 121656.
[35] V. Ganesan, R. Patel, J. Hartwig, I. Mudawar, Universal correlations for post-CHF saturated and superheated flow film boiling heat transfer coefficient, minimum heat flux and rewet temperature for cryogenic fluids in uniformly heated tubes, Int. J. Heat Mass Transfer 195 (2022), 123054.
[36] S.M. Kim, I. Mudawar, Universal approach to predicting two-phase frictional pressure drop for adiabatic and condensing mini/micro-channel flows, Int. J. Heat Mass Transfer 55 (2012) 3246–3261.
[37] S.M. Kim, I. Mudawar, Universal approach to predicting two-phase frictional pressure drop for mini/micro-channel saturated flow boiling, Int. J. Heat Mass Transfer 58 (2013) 718–734.
[38] W.H. McAdams, W.K. Woods, L.C. Heroman, Vaporization inside horizontal tubes, II. Benzene–oil mixture, Trans. ASME 64 (1942) 193–200.
[39] W.W. Akers, H.A. Deans, O.K. Crosser, Condensing heat transfer within horizontal tubes, Chem. Eng. Prog. 54 (1958) 89–90.
[40] A. Cicchitti, C. Lombardi, M. Silvestri, G. Soldaini, R. Zavalluilli, Two-phase cooling experiments-pressure drop, heat transfer and burnout measurements, Energia nucleare 7 (1960) 407–425.
[41] W.L. Owens, Two-phase pressure gradient. Int. Dev. Heat Transfer, Pt. II., ASME, New York, 1961.
[42] A.E. Dukler, M. Wicks, R.G. Cleaveland, Pressure drop and hold up in two-phase flow, AIChE J. 10 (1964) 38–51.
[43] S. Lin, C.C.K. Kwok, R.Y. Li, Z.H. Chen, Z.Y. Chen, Local frictional pressure drop during vaporization of R-12 through capillary tubes, Int. J. Multiph. Flow 17 (1991) 95–102.
[44] D.R.H. Beattie, P.B. Whalley, A simple two-phase frictional pressure drop calculation method, Int. J. Multiph. Flow 8 (1982) 83–87.
[45] R.W. Lockhart, R.C. Martinelli, Proposed correlation of data for isothermal two phase, two-component flow in pipes, Chem. Eng. Prog. 45 (1949) 39–48.
[46] L. Friedel, Improved Friction Pressure Drop Correlations For Horizontal and Vertical Two-Phase Pipe Flow, European Two-phase Group Meeting, Ispra, Italy, 1979. Paper E2.
[47] H. Müller-Steinhagen, K. Heck, A simple friction pressure drop correlation for two-phase flow in pipes, Chem. Eng. Process. 20 (1986) 297–308.
[48] S.M. Kim, I. Mudawar, Review of databases and predictive methods for pressure drop in adiabatic, condensing and boiling mini/micro-channel flows, Int. J. Heat Mass Transf. 77 (2014) 74–97.
[49] A.J. Ghajar, S.M. Bhagwat, Effect of void fraction and two-phase dynamic viscosity models on prediction of hydrostatic and frictional pressure drop in vertical upward gas–liquid two-phase flow, Heat Transf. Eng. 34 (2013) 1044–1059.
[50] S.M. Zivi, Estimation of steady-state steam void-fraction by means of the principle of minimum entropy production, J. Heat Transfer 86 (1964) 247–252.
[51] D.H. Pope, W.R. Killian, R.J. Corbett, Single-Phase Flow Tests with Liquid Hydrogen, Adv. Cryog. Eng. 5 (1960) 441–449.
[52] J.H. Jones, M. Altman, Two-phase flow and heat transfer for boiling liquid nitrogen in horizontal tubes, In Chem. Eng. Prog. Symp. Ser. 61 (1965) 205–212.
[53] V.E. Keilin, E.Ju. Klimenko, I.A. Kovalev, B.N. Samoilov, Force-cooled superconducting systems, Cryogenics 10 (1970) 224–232 (Guildf).
[54] A. de La Harpe, S. Lehongre, J. Mollard, C. Johannès, Boiling heat transfer and pressure drop of liquid helium-I under forced circulation in a helically coiled tube, Adv. Cryog. Eng. 14 (1969) 170–177.
[55] M. Jergel, R. Stevenson, Heat transfer to liquid helium in narrow channels with laminar and turbulent flow, Appl. Phys. Lett. 17 (1970) 125–127.

[56] M. Jergel, K. Hechler, R. Stevenson, The effect of forced circulation on heat transfer with liquid helium in narrow channels, Cryogenics 10 (1970) 413–417 (Guildf).
[57] D. Steiner, E.U. Schlünder, Heat transfer and pressure drop for boiling nitrogen flowing in a horizontal tube. 2. Pressure drop, Cryogenics 16 (1976) 457–464 (Guildf).
[58] D. Steiner, E.U. Schlünder, Heat Transfer and Pressure Drop For Boiling Nitrogen Flowing in a Horizontal Tube, Hemisphere Publishing Corporation, New York, 1977, pp. 263-306.
[59] V.I. Deev, Yu.V. Gordeev, A.I. Pridantsev, V.I. Petrovichev, V.V. Arkhipov, Hydraulic resistance to forced two-phase flow of helium in narrow channels, Soviet Atomic Energy 42 (1977) 381–383.
[60] H.K. Zust, Flow Boiling in Liquid Helium, Oxford University, 1978. Ph.D. Thesis.
[61] V.I. Deev, Yu.V. Gordeev, A.I. Pridantsev, V.I. Petrovichev, V.V. Arkhipov, Pressure drop in a two-phase flow of helium under adiabatic conditions and with heat supply, in: Proceedings of the International Heat Transfer Conference Digital Library, 1978.
[62] B.S. Petukhov, V.M. Zhukov, V.M. Shieldcret, Investigation of heat transfer and hydrodynamics in the helium two-phase flow in a vertical channel, in: Advanced Course in Heat Exchangers: Theory and Practice, ICHMT Symposium, 1981, pp. 251–262.
[63] H.M. Müller, W. Bonn, D. Steiner, Flow boiling heat transfer and pressure drop of nitrogen from 1 to 30bar. Proceedings of the 20th International Cryogenic Engineering Conference, 1982, pp. 69–72.
[64] I.P. Vishnev, L.N. Migalinskaya, I.B. Lebedeva, Experimental study of the drag of a two-phase helium flow in channels, J. Eng. Phys. 43 (1982) 841–846.
[65] I.S. Mamedov, V.M. Miklyaev, V.I. Pryanichnikov, Yu.P. Filippov, Hydrodynamic characteristics of a horizontal channel with the motion of a two-phase helium flow, J. Eng. Phys. 44 (1983) 483–486.
[66] S.Z. Gan, Yu.P. Filippov, Calculation of hydraulic resistance of channels for two-phase helium flow, Teploenergetika 31 (1984) 19–23.
[67] V.I. Subbotin, V.I. Deev, A.I. Pridantsev, V.K. Andreev, V.V. Arkhipov, V. N. Novikov, A.N. Savin, V.V. Solodovnikov, Heat transfer and hydrodynamics in cooling channels of superconducting devices, Cryogenics 25 (1985) 261–265 (Guildf).
[68] V.I. Subbotin, V.I. Deev, V.V. Solodovnikov, V.V. Arkhipov, Heat transfer in two-phase flow of helium, Int. Heat Transfer Conf. (1986) 2343–2348. Digital Library.
[69] M. Popp, D. Preclik, Two-phase flow in cryogenic rocket engine feed systems, in: Proceeding of the In 25th Joint Propulsion Conference, 1989. AIAA-89-2392.
[70] R.C. Hendricks, R.W. Graham, Y.Y. Hsu, R. Friedman, Experimental heat transfer and pressure drop of film boiling liquid hydrogen flowing through a heated tube, National Aeronautics and Space Administration Technical Note D-765, 1961.
[71] X. Huang, S.W. Van Sciver, Pressure drop and void fraction of two-phase helium flowing in horizontal tubes, Cryogenics 35 (1995) 467–474 (Guildf).
[72] X. Huang, Hydrodynamic Study of One Dimensional Two-Phase Helium Flow, The University of Wisconsin-Madison, 1994. Ph.D. Thesis.
[73] Yu.P. Filippov, Characteristics of horizontal two-phase helium flows. Part II: pressure drop and transient heat transfer, Cryogenics 39 (1999) 69–75 (Guildf).
[74] S.L. Qi, P. Zhang, R.Z. Wang, L.X. Xu, Flow boiling of liquid nitrogen in micro-tubes: part I–The onset of nucleate boiling, two-phase flow instability and two-phase flow pressure drop, Int. J. Heat Mass Transf. 50 (2007) 4999–5016.
[75] T. Rane, A. Chakravarty, R.K. Singh, T. Singh, Improved correlations for computations of liquid helium two phase flow in cryogenic transfer lines, Cryogenics 51 (2011) 27–33 (Guildf).
[76] S. Mustafi, High Reynolds number Vertical Up-Flow Parameters For Cryogenic Two-Phase Helium I, University of Maryland, 2014. Ph.D. Thesis.
[77] D. Deng, S.W. Xie, X.D. Li, R.S. Wang, Flow boiling heat transfer of liquid nitrogen in heated U-tubes, J. Heat Transf. 136 (2014), 024501.
[78] N. Dittmar, Ch. Haberstroh, U. Hesse, M. Krzyzowski, Characterization and optimization of flexible transfer lines for liquid helium. Part I: experimental results, Cryogenics 75 (2016) 6–12 (Guildf).
[79] M.H. Chang, M.H. Tsai, Ch. Wang, M.C. Lin, F.T. Chung, M.S. Yeh, L.H. Chang, C. H. Lo, T.C. Yu, L.J. Chen, Z.K. Liu, Pressure drop of two-phase helium along long cryogenic flexible transfer lines to support a superconducting RF operation at its cryogenic test stand, Spring. Plus 5 (2016) 2077.
[80] X. Chen, S. Chen, J. Chen, J. Li, X. Liu, L. Chen, Y. Hou, Two-phase flow boiling frictional pressure drop of liquid nitrogen in horizontal circular mini-tubes: experimental investigation and comparison with correlations, Cryogenics 83 (2017) 85–94 (Guildf).
[81] R.C. Hendricks, R.W. Graham, Y.Y. Hsu, R. Friedman, Experimental heat-transfer results for cryogenic hydrogen flowing in tubes at subcritical and supercritical pressures to 800 pounds per square inch absolute, NASA Tech. (1966). Note D-3095.
[82] V. Mohr, R. Runge, Forced Convection Boiling of Neon in Horizontal Tubes, Hemisphere, New York, 1977, pp. 307-343.
[83] B.C. Huang, Q.L. Li, Y. Wang, J.Q. Zhang, J. Song, F.C. Zhuang, Experimental investigation of nitrogen flow boiling heat transfer in a single mini-channel, J. Zhejiang Univ. Science A 21 (2020) 147–166.
[84] A.K.H. Khalil, Cryogenic Two-Phase Flow Characteristics of Helium I in Vertical Tubes, University of Wisconsin-Madison, 1978. Ph.D. Thesis.
[85] W.F. Laverty, W.M. Rohsenow, Film Boiling of Saturated Liquid Flowing Upward Through a Heated tube: High Vapor Quality Range, Massachusetts Institute of Technology, Heat Transfer Laboratory, 1964. Technical Report 9857-32.
[86] R.P. Forslund, W.M. Rohsenow, Thermal non-equilibrium in dispersed flow film boiling in a vertical tube, Massachusetts Institute of Technology, Heat Transfer Laboratory, Tech. Rep. 44 (1966).
[87] J. Lee, I. Mudawar, Fluid flow and heat transfer characteristics of low temperature two-phase micro-channel heat sinks – Part 2: subcooled boiling pressure drop and heat transfer, Int. J. Heat Mass Transf. 51 (2008) 4327–4341.
[88] T.J. LaClair, I. Mudawar, Thermal transients in a capillary evaporator prior to the initiation of boiling, Int. J. Heat Mass Transf. 43 (2000) 3937–3952.
[89] S. Mukherjee, I. Mudawar, Pumpless loop for narrow channel and micro-channel boiling from vertical surfaces, J. Electron. Packag. 125 (2003) 431–441.
[90] M.K. Sung, I. Mudawar, Single-phase and two-phase heat transfer characteristics of low temperature hybrid micro-channel/micro-jet impingement cooling module, Int. J. Heat Mass Transf. 51 (2008) 3882–3895.
[91] L.E. O'Neill, I. Mudawar, Review of two-phase instabilities in macro- and micro-channel systems, Int. J. Heat Mass Transf. 157 (2020), 119738.